Presence and geodynamic significance of Cambro-Ordovician series of SE Karakoram (N Pakistan)

Yann Rolland [a,*], Christian Picard [a,b], Arnaud Pêcher [a], Elisabeth Carrio [a], Simon M.F. Sheppard [c], Massimo Oddone [d], Igor M. Villa [e]

[a]*LGCA-LGIT, UMR-A5025 CNRS - Université J. Fourier, Maison des Géosciences, B.P. 53, 38041 Grenoble, France*
[b]*Université de Nouvelle-Calédonie, BP 4477, Géosciences, 98847 Nouméa, New Caledonia*
[c]*UMR 8515, Ecole Normale Supérieure de Lyon, Allée d'Italie, F-69364, Lyon, France*
[d]*Universita di Pavia, Dipartimento di Chimica Generale, via Taramelli 12, 27100 Pavia, Italy*
[e]*Isotopengeologie, Erlachstrasse 9a, 3012 Bern, Switzerland*

Abstract

New geological, geochemical and geochronological data from the Southern Karakoram (NE Pakistan) indicate the presence of several unexpectedly old and well preserved units along the Asian margin: (1) a Precambrian basement, displaying a minimum amphibole Ar-Ar age of 651 Ma; (2) a thick Cambro-Ordovician platform-type sedimentary unit overlying the Precambrian basement. These series are dated by graptolite and crinoid faunas, and are confirmed by concordant $^{87}Sr/^{86}Sr$ and ^{13}C "ages" of the marbles; (3) a dismembered ophiolitic series formed by slices of metagabbros and metabasalts separated by ultramafic lenses (the Masherbrum Greenstone Complex). The occurrence of such Cambro-Ordovician series overlying a Precambrian basement in south-eastern Karakoram similar to the south-western Karakoram shows that the Karakoram constitutes a continuous tectonic block. The petrology and geochemistry of the Masherbrum Greenstone Complex (mineral chemistry, major and trace element and Sr-Nd isotopic data) are indicative of a supra-subductive environment. The presence of LREE-enriched calc-alkaline rocks [$(La/Yb)_N = 4.4$-5.6; $(Nb/La)_N = 0.2$-0.3; $\varepsilon Nd_{565} = 5.1$-$7.1$] and LREE-depleted tholeiitic rocks [$(La/Yb)_N = 0.5$-1.3; $(Nb/La)_N = 0.6$-0.9; $\varepsilon Nd_{565} = 5.6$-$7.8$] are consistent with arc and back-arc settings, respectively. A high-Mg andesitic dolerite and an OIB-type metabasalt, with lower εNd ratios ($\varepsilon Nd_{565} = 0.5$ and 4.5) are in accordance with source heterogeneity beneath the arc. The Masherbrum Greenstone Complex, along with other Cambro-Ordovician central-eastern volcanic series give evidence of a tectonic situation governed by micro-plate convergent-divergent systems with occurrence of arc - back-arc settings during the Lower Palaeozoic, comparable to that of the current SW Pacific area. © 2002 Éditions scientifiques et médicales Elsevier SAS. All rights reserved.

Keywords: Karakoram; Cambrian-Ordovician; Arc; Back-arc; Isotopes; Accretion

1. Introduction

Since Early Palaeozoic, continuous plate tectonics, involving closure of oceanic domains, crustal aggregation of numerous micro-plates and mountain building occurred in the central-eastern Asian realm resulting in the present day Himalayan mosaic. One of the puzzling problems concerns the Palaeozoic geodynamic setting of certain parts of this mountain belt. The Karakoram, located in a central tectonic position of central-eastern Asian blocks (Fig. 1), is a key region for a better understanding of the geodynamics of Central-Eastern Asian Blocks during the Lower Palaeozoic.

The south-western part of the Karakoram (north-west Pakistan) has revealed the presence of Ordovician to Triassic series resting on a Pre-Arenigian (> 465 Ma) basement [1–3]. The northern Karakoram region has revealed Permian to Jurassic rocks, starting with Lower Permian terrigenous alluvial material, covered by Upper Permian and Triassic carbonate peritidal-type carbonate formations and ending up with Liassic molasse layers and shallow Upper Jurassic marine carbonates [4,5]. However, the age and geodynamic evolution of the south-eastern Karakoram margin remains

---

* Corresponding author.
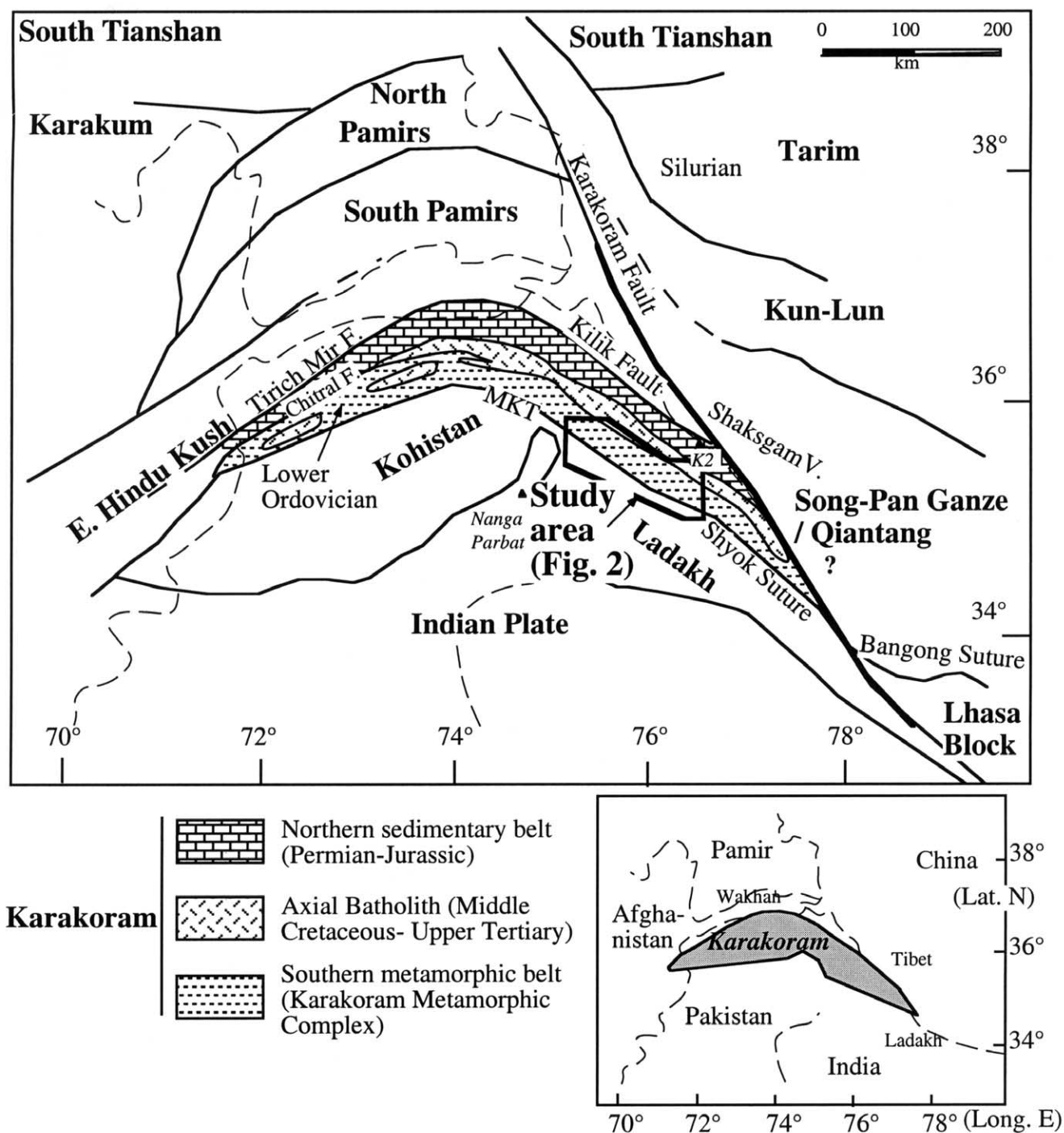 *E-mail address:* yrolland@ujf-grenoble.fr (Y. Rolland).

Fig. 1. Schematic map of the Pamir-Karakoram syntaxis, with location of principal tectonic blocks and sutures. The main geological units of Karakoram are shown. The location of studied area in south-eastern Karakoram is indicated. MKT: Main Karakoram Thrust.

poorly documented, due to a strong Tertiary metamorphic overprint in this area since the Eocene India-Asia collision (~ 50 Ma) up to Pliocene (~ 9 Ma). This metamorphism culminates with amphibolite to granulite facies conditions and an important plutonism in the Braldu Valley, Askole area [6–10], Fig. 2. This part of the Karakoram is currently thought to be the southern equivalent of Upper Palaeozoic

northern Karakoram series [11]. However, a lower metamorphic grade area is exposed from the upper Thalle Valley in the south, along the Shyok Suture Zone, to the Masherbrum Peak in the north [7]. This lower grade area has seen little geological attention in the recent past, but was pioneered by geologists at the end of the nineteenth century. Initial investigators of the area noted the presence of
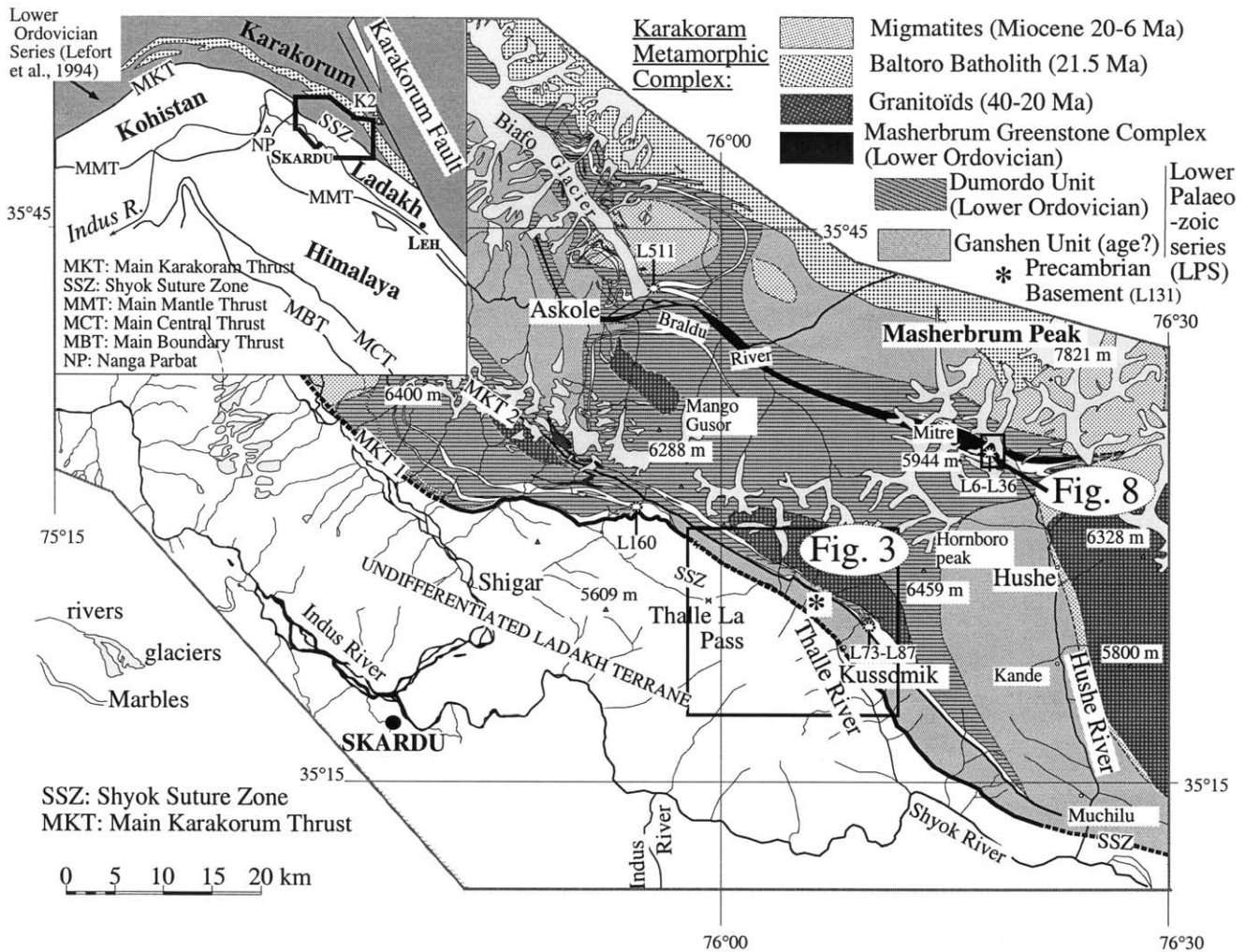
Fig. 2. Geological map of the Karakoram Metamorphic Complex (Skardu area - NE Pakistan), with locations of the samples of Tables I and II and those of Figs 3 and 8.

fossiliferous limestones on the southern slope of the Masherbrum Peak, with echinoderms of the genus *Sphaeronites* that they attributed to the Silurian [12,13]. Although these ages were subsequently used in regional reconstitutions [14–16], the fossils were never described in more detail. Further, the Masherbrum formations were attributed a Permo-Carboniferous age on the basis of sediment facies analyse [17]. Over the past thirty years no bio-stratigraphic constraints have been provided for the Palaeozoic protolith of the Karakoram, and the Silurian fossils were not taken into account [18,19].

The purpose of this work is to provide further constrains on the pre-Himalayan history of the Karakoram margin and to attempt to integrate it in the geodynamic history of central-eastern Asian blocks during the Lower Palaeozoic. We focus on the lower grade metamorphic zone of southeastern Karakoram, from Upper Thalle Valley to the southern edge of the Masherbrum Peak (Fig. 2). Age constrains are provided by both palaeontological and isotopic (Sr, Nd, Ar, C) chronometers. The geodynamic setting is reconsti-

tuted using geological and geochemical analyse of sedimentary and magmatic rocks, and their comparison with current settings.

2. Geological setting

The limits of the Karakoram block (Fig. 1) are still only approximately defined. The western limit of Karakoram with east Hindu Kush is proposed along the Tirich Mir fault or the Chitral fault where serpentinized ultramafic rocks have been found [3,20]. To the north, the boundary with south Pamirs is poorly defined, as access to the Wakhan part of Afghanistan is still difficult for political reasons. But a limit along the Kilik fault has been proposed [21,22], as this fault thrusts Permo-Carboniferous sediments over northern Karakoram Cretaceous sediments, and can be followed westwards to the western Karakoram [23,24]. Terrains located on the eastern side of the Karakoram Fault have been included in the Karakoram s.l. by several authors

Table I

Geochemical analyses of Precambrian Basement and of representative rocks of the Masherbrum Greenstone Complex.

Unit	Masherbrum Complex								P.B.
Sample N°.	L10	L4	L12	L36	L28	L27	L20	L13	L131
Lithology	gabbro	B andesite	diorite	gabbro	gabbro	diorite	basalt	high-Mg and.	High-Mg
Type	Arc type			Back-Arc type			OIB-type	dolerite	diorite
Major elements (wt%-normalised to 100%)									
SiO_2	51,06	53,92	58,24	50,80	53,74	60,43	49,57	56,50	57,85
TiO_2	0,69	0,78	0,81	0,33	0,87	1,00	3,54	0,36	0,77
Al_2O_3	17,09	17,16	16,76	16,74	17,32	15,02	14,17	13,60	14,42
Fe_2O_3	1,59	1,46	1,35	1,10	1,60	1,48	2,12	1,25	1,15
FeO	8,11	7,44	6,89	5,60	8,17	7,54	10,81	6,35	5,88
MnO	0,52	0,16	0,13	0,13	0,12	0,12	0,13	0,16	0,15
MgO	7,40	5,67	4,17	10,80	6,36	4,53	8,33	8,92	8,57
CaO	10,82	10,26	9,00	12,35	8,15	5,14	8,85	9,68	6,99
Na_2O	2,44	2,68	2,27	1,99	3,26	4,24	1,94	2,97	2,69
K_2O	0,15	0,26	0,22	0,12	0,35	0,42	0,07	0,20	1,33
P_2O_5	0,11	0,20	0,16	0,04	0,07	0,08	0,47	0,02	0,17
LOI	0,80	0,65	0,34	1,44	1,35	0,70	8,88	0,74	2,12
Trace elements (ppm)									
Ba	53	73	43	12	30	24	36	39	424
Rb	0,86	3,63	5,43	4,67	6,56	6,34	1,40	1,86	34,35
Sr	365	458	528	117	225	139	404	126	386
Ta	0,12	0,19	0,57	0,04	0,23	0,11	1,61	0,32	0,14
Th	1,82	3,43	4,03	0,13	0,59	0,32	2,94	2,54	0,86
Zr	80	83	130	26	79	70	230	52	86
Nb	1,6	2,4	4,0	0,5	2,7	1,1	26,4	3,9	1,8
Y	15,30	20,07	22,45	13,74	26,30	18,78	27,65	15,26	9,74
Hf	0,57	1,08	0,51	0,31	0,31	0,40	0,63	0,32	0,46
Cr	107	59	28	308	23	22	254	15	11
Ni	46	28	14	96	61	9	211	125	63
Co	72	62	46	48	92	45	69	469	578
U	0,756	1,125	1,370	-	0,173	0,082	0,647	0,614	0,173
Pb	13,04	7,86	7,38	4,31	9,40	1,80	6,90	4,91	5,97
Cs	0,06	1,25	1,55	1,79	1,69	1,64	0,34	0,23	0,77
La	8,01	14,53	14,35	0,74	3,27	1,85	26,78	5,88	10,28
Ce	17,92	29,56	29,83	2,15	7,83	5,07	62,16	12,20	22,69
Pr	2,36	3,83	3,68	0,38	1,18	0,83	8,22	1,39	2,84
Nd	10,35	16,73	14,83	2,13	5,70	4,53	36,48	5,34	12,06
Sm	2,70	4,06	3,58	0,89	1,94	1,72	8,72	1,43	2,65
Eu	0,785	1,239	0,976	0,354	0,795	0,425	2,738	0,606	1,024
Gd	2,60	3,88	3,46	1,09	2,13	2,03	7,83	1,59	2,73
Tb	0,432	0,617	0,551	0,236	0,425	0,435	1,173	0,276	0,323
Dy	2,41	3,32	3,48	1,70	3,04	2,82	5,66	1,87	1,76
Ho	0,497	0,675	0,780	0,409	0,709	0,608	0,993	0,441	0,370
Er	1,43	1,97	2,03	1,10	1,89	1,85	2,47	1,17	0,90
Yb	1,235	1,742	1,882	1,071	1,764	1,757	1,686	1,157	0,764
Lu	0,185	0,257	0,276	0,165	0,268	0,256	0,229	0,181	0,118
$(La/Sm)_{Chondrite-N}$	2,3	2,5		1,1	0,7		2,6		
$(La/Yb)_{Chondrite-N}$	5,6	5,2		1,3	0,7		3,4		
Mg#	0,58	0,54	0,48	0,75	0,54	0,48	0,54	0,68	0,69
Isotopic ratios:									
$^{143}Nd/^{144}Nd$	-	0.512713±8	0.512751±10	0.513037±9	0.512969±11	0.513039±5	0.512689±3	0.512538±11	-
$(^{143}Nd/^{144}Nd)_{565}$	-	0,51217	0,51227	0,51220	0,51229	0,51231	0,51214	0,51194	-
$\varepsilon(Nd)_{565}$	-	5,09	7,12	5,59	7,39	7,83	4,52	0,54	-
$^{147}Sm/^{144}Nd$	-	0,14656	0,12880	0,22713	0,18397	0,19678	0,14453	0,16228	-
$^{87}Sr/^{86}Sr$	-	0.705246±9	0.705432±30	0.704846±21	0.706582±19	-	-' (*)	0.706750±25	-
$(^{87}Sr/^{86}Sr)_{565}$	-	0,70506	0,70519	0,70392	0,70590	-	-	0,70641	-
$\varepsilon(Sr)_{565}$	-	17,44	19,30	1,18	29,40	-	-	36,53	-

P.B.: Precambrian Basement; B andesite: Basaltic andesite; and: andesite

(*): not determined due to elevated LOI

Table II
Isotopic compositions of Karakorum and Ladakh marbles.

	$\delta^{13}C_{PDB}$	$^{87}Sr/^{86}Sr$
Karakorum		
L511(Askole)	3,05	
L6 (Masherbrum)	3,82	
L160 (Bauma Harel)	3,1	
L77 (Upper Thalle)	4	
L76 (Upper Thalle)	1,06	
L73 (Upper Thalle)	-0,07	
L87b (Upper Thalle)	-0,24	0.70906±1
Shyok Suture (Ladakh)		
L391		0.70745±2
L427		0.70718±1

[25–28]. But this interpretation is still debated, as Gaetani et al. [4,29] proposed that the sedimentary successions of the Shaksgam Valley could belong to the south Pamirs, as also supported by descriptions of the Qiantang area by Sun [30]. To the south, the boundary with the Ladakh Terrain is a complex suture zone closed in the upper Cretaceous (the Shyok Suture Zone) and reactivated during the Tertiary (Main Karakoram Thrust) [31–34,11].

The Karakoram is composed of two east-west striking belts separated by the axial batholith of Mid-Cretaceous to Upper Tertiary age [35]. The northern sedimentary belt is formed by Permian to Jurassic slates and limestones [4,5,22]. The southern Karakoram belt is known as the Karakoram Metamorphic Complex [7,36]. In the southeastern Karakoram (Skardu area, Fig. 2), the Karakoram Metamorphic Complex is mainly comprised of metasediments, which have been divided into the Ganshen Formation (paragneisses and subordinate marbles) and the Dumordo Unit (principally marbles and marls; [37]), and of several orthogneisses. A minor proportion of amphibolites and metabasites occurs from Askole in the West, to the upper Hushe Valley (south of the Masherbrum Peak). This last series, referred to as the Panmah ultramafic-mafic unit by Searle et al. [7,38], and presumed to be a Mesozoic suture remnant by these authors, or to represent the Shyok Suture Zone volcanics folded into the southern Karakoram margin [6]. This unit is better preserved South of the Masherbrum Peak, where it shows slices of different magmatic origins, together with minor ultramafic interlayers; consequently we prefer the name of Masherbrum Greenstone Complex to that of Panmah ultramafic-mafic unit.

These units were intensely deformed during the Himalayan orogeny, which started with the collision of Indian and Asian plates at ~ 50 Ma [33,34,39,40]. The tectonic style during the 50-20 Ma period corresponds to the stacking of a poly-metamorphic pile in a north-west – south-east striking, south vergent, compressive context, associated with intense isoclinal folding [7,9]. The Shyok Suture Zone has been reactivated mainly in its western Kohistan side, where it is called the MKT (Main Karakoram Thrust). During this period, a first phase of magmatism occurred with the intrusion of Mango Gusor type granites, the Mango Gusor pluton being dated to 37-26 Ma [41,42]. The phase of plutonism culminated with the intrusion of the large Baltoro Batholith at 21-25 Ma [41,43]. During the later period (20-6 Ma), intense migmatization and granulite facies metamorphism developed along the Braldu Valley (Fig. 2), linked to the development of a thermal anomaly [9,10].
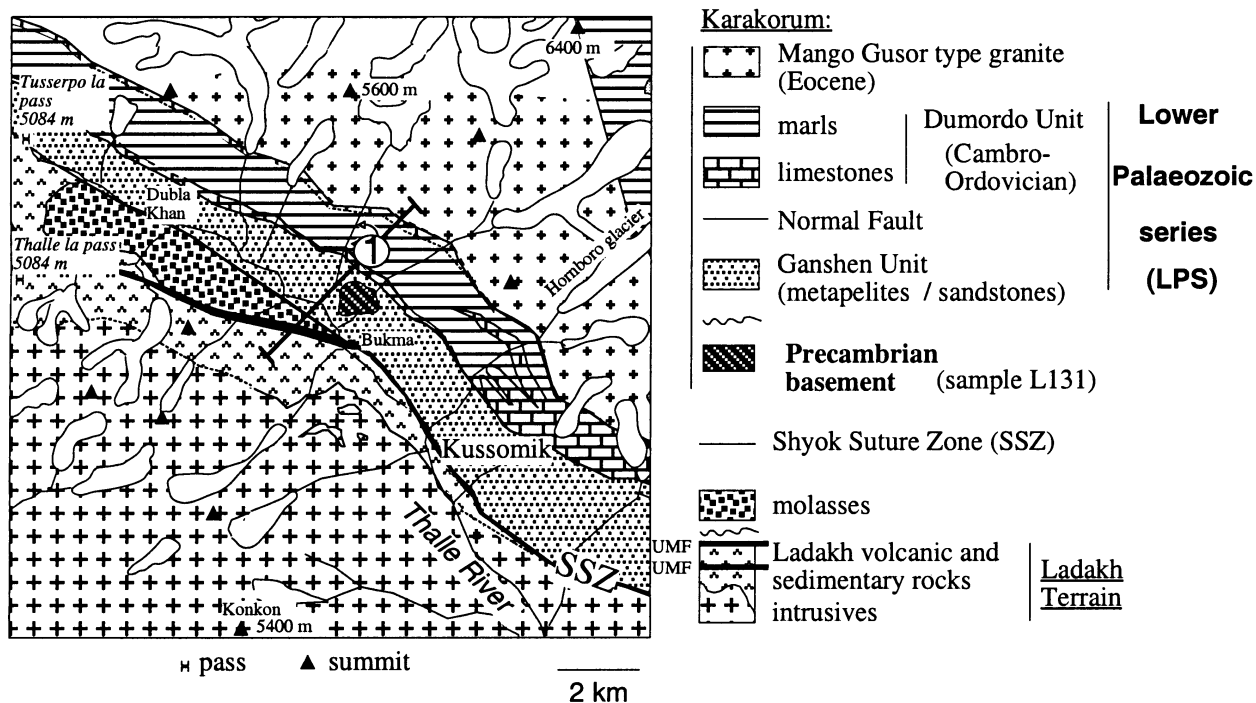

Fig. 3. Geological map of the southern Karakoram Margin and Shyok Suture Zone in the Upper Thalle Valley (location on Fig. 1). 1: cross-section of Fig. 4.
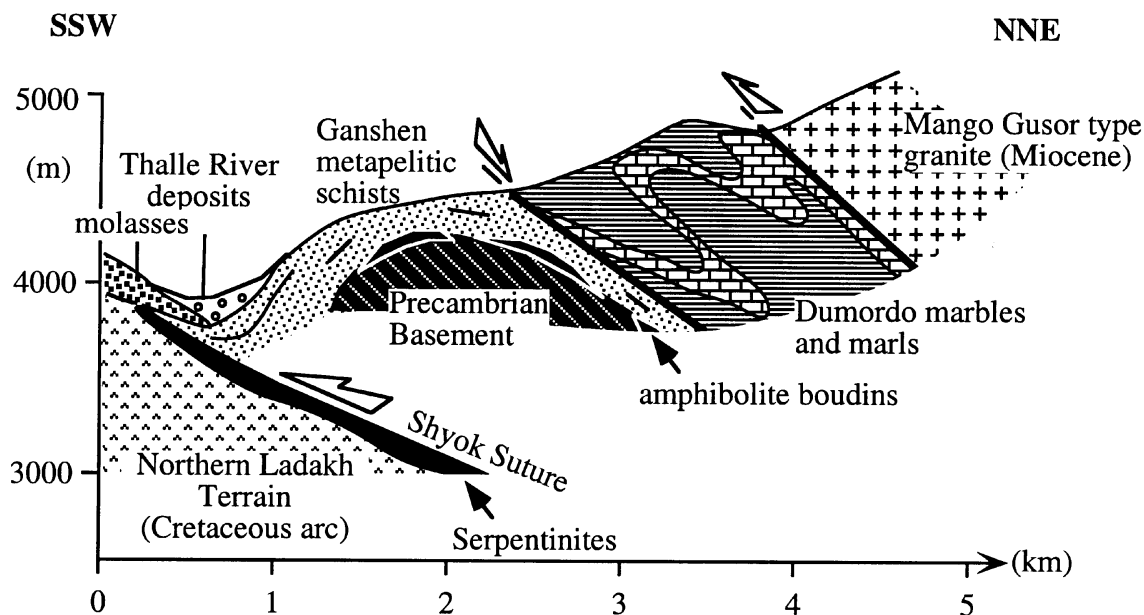
Fig. 4. Cross-section of the Southern Karakoram margin in the Upper Thalle Valley. For location of the section and nature of symbols, see Fig. 3.

3. Results

3.1. The Precambrian basement

The Precambrian basement outcrops in a kilometre large window on the northern side of the Shyok Suture in the Upper Thalle Valley, near the village of Kussomik (Figs 3 and 4). It appears in the core of an anticline, on the northern limb of the Shyok Suture, overlaid by Lower Palaeozoic pelitic series (see § 3.2). The contact between the Precambrian basement and the Lower Palaeozoic series is discontinuous and underlined by a boudinaged amphibolite layer (Fig. 4). The basement (sample L131) is a mildly foliated metadiorite, which in thin section consists of centimetre large magnesio-hornblende / pargasite and plagioclase crystals (An 20-30) with abundant accessory phases (sphene, apatite and magnetite) metamorphosed in the greenschist facies with minor occurrence of chlorite at the rim of the amphibole or in the matrix. Microprobe analyses of amphibole grains show a progressive substitution of a pargasitic edenite core, with a Ca/K of ~ 20 by magnesio-hornblende towards the rim showing a Ca/K of ~ 15.

Ar-Ar spectra of the amphibole separate of sample L131 is presented on Fig. 5A. It displays a staircase age spectrum from the lower temperature step (703°C; 166 Ma) to the higher temperature step (1287°C; 651 Ma). Age and Ca/K ratio are positively correlated (Fig. 5B). This discordant argon spectrum is interpreted to reflect important Ar loss from amphibole through recrystallisation during greenschist grade Himalayan metamorphism. We believe that, as already proposed for some metabasites from the Shyok Suture Zone by Villa et al. [44], the higher Ca/K ratios displayed by the older age steps of the Ar-Ar spectrum reflect the contribution of the amphibole core. Recent systematisations of age-chemistry correlations are given by [45,46]. The core would probably represent the magmatic stage, whereas the rim would represent metamorphic reequilibration. In particular, the very low Ca/K values of the lower age steps (0-7) are due to the contribution of phyllosilicates that are finely intergrown at amphibole rims. Consequently, the age of 651 Ma may be considered as a minimum age for the Precambrian basement in regard to Ar loss of the amphibole core.

The geochemical analyses of sample L131 are presented in Table I and Fig. 6. L131 is a high-Mg diorite, with similar major element contents as current Mg-rich andesites [48–49]. L131 has mafic characteristics including high Mg # (Mg/Mg+Fe^{2+} = 0.72), elevated $Fe_2O_3 + MgO + TiO_2 + MnO$ (10.7 wt%) and relatively high Ni and Cr contents (63 and 11 ppm, respectively), for such a SiO_2 content. In spite of this mafic character, L131 displays a marked negative Nb-Ta anomaly [(Nb/La)$_{MORB-N}$ = 0.2], typical of arc lavas. Further, it displays low HREE contents (Yb = 0.76 ppm) and a relatively high Sr content (385 ppm), similar to those of current adakitic lavas [e.g., 50]. These compositions are therefore transitional between adakites and typical calc-alkaline arc lavas. Such compositions are currently found in volcanic arc settings [51]. Adakites require elevated temperature conditions in the source region, and are likely produced by subducted slab melting and interaction with overlying mantle (e.g., [51–53]). Consequently, such geochemical compositions are suggestive of a supra-subductive setting and a high geothermal gradient.
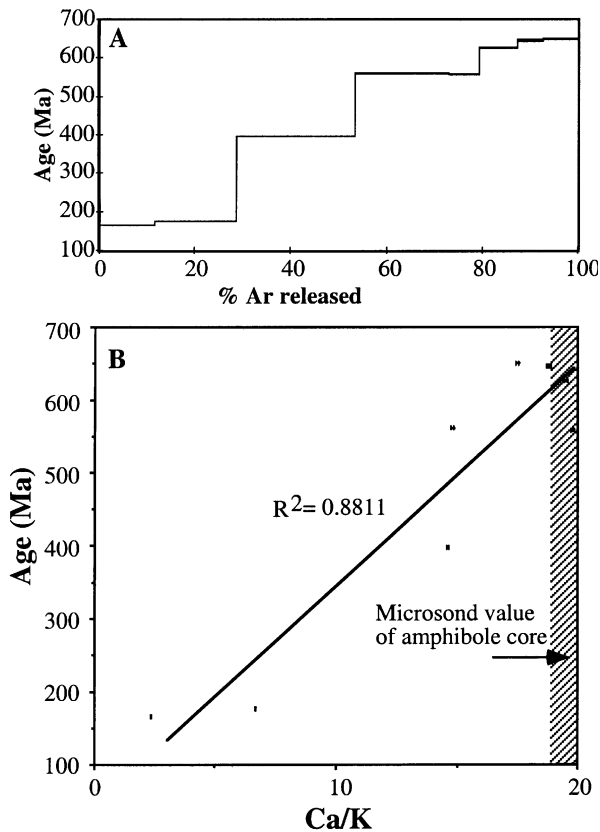
Fig. 5. A, Ar-Ar spectra of L131 hornblende separate. B, Ca/K vs. age diagram (calculated from the data obtained with the rare gas spectrometer). The Ca/K ratio of amphibole core, obtained with a microprobe, has also been shown. Note the good fit of amphibole core Ca/K microprobe ratio value with older steps (651 Ma) Ca/K ratio values.

3.2. The Lower Palaeozoic series

In the Upper Thalle Valley, the basal part of the Lower Palaeozoic series is a thick layer of metapelites and sandstones or quartz-arenites overlying the Precambrian basement (Figs 3 and 4), and forming a 2500 - 3500 m-thick band parallel to the Shyok Suture. The mainly silico-clastic nature of this basal part resembles the Ganshen Unit and Hushe gneisses [7]. In the metapelitic lithologies, the assemblage: muscovite + biotite + quartz ± K-feldspar corresponds to greenschist facies metamorphic conditions. This basal part of the Lower Palaeozoic series is structurally overlain by a folded sequence of marls and limestones (upper part). The contact between the two parts is a north dipping extensive fault (Fig. 4). The mineralogical nature of the upper part shows lower metamorphic grade assemblages (calcite, smectite/chlorite, quartz ± phengite). The mainly carbonaceous nature of this upper part looks similar to the Dumordo Unit described by Desio and Searle [7,37]. The limestones contain abundant palaeontological faunas, mainly graptolite and crinoid clasts, mixed with rounded quartz grains (≤ 5 mode-%), defining a detrital platform-type environment. The graptolites are of the type *Dictyonema flabelliform*, characteristic of the Lower Ordovician.

In parallel to this palaeontological age, we also used complementary methods of dating.

- We measured the isotopic $^{87}Sr/^{86}Sr$ ratio of a pure marble bearing graptolites and crinoids (L87), of the low-grade metamorphic zone (Table II). This ratio, plotted on the Sr isotope evolutionary curve of seawater versus time [54], yields an age of ~ 500 Ma (Fig. 7a), at
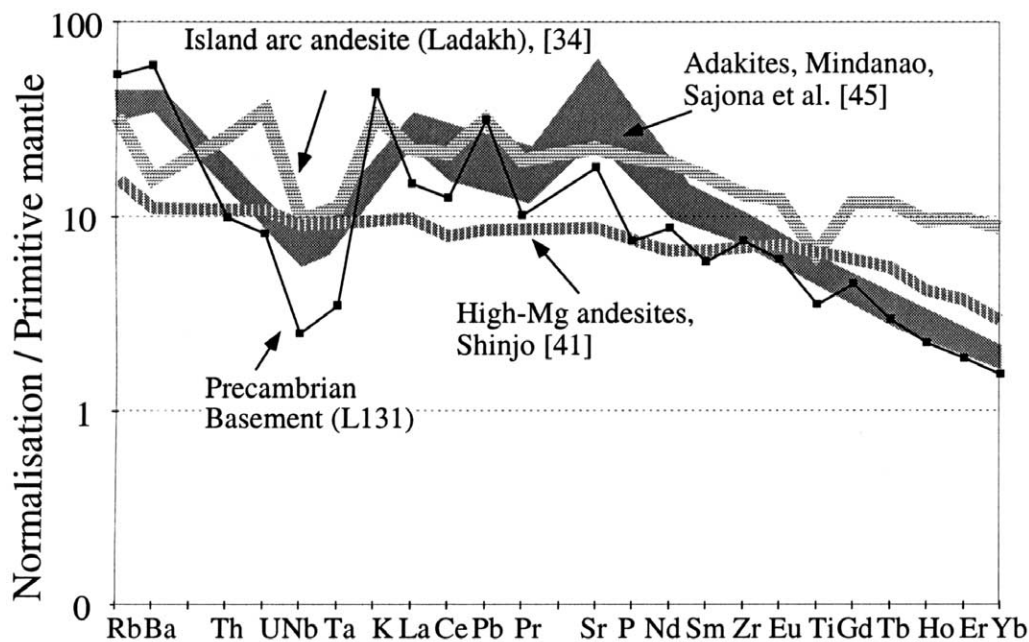

Fig. 6. Primitive mantle-normalised element pattern of Precambrian Basement (sample L131, filled boxes). Patterns of adakites [52], high-Mg andesites [49] and of a typical (Ladakh) island arc andesite [34] are shown for comparison. Note the good fit of L131 and adakites, except a deeper Nb-Ta negative anomaly. Normalisation values are those of Sun & McDonough [47].
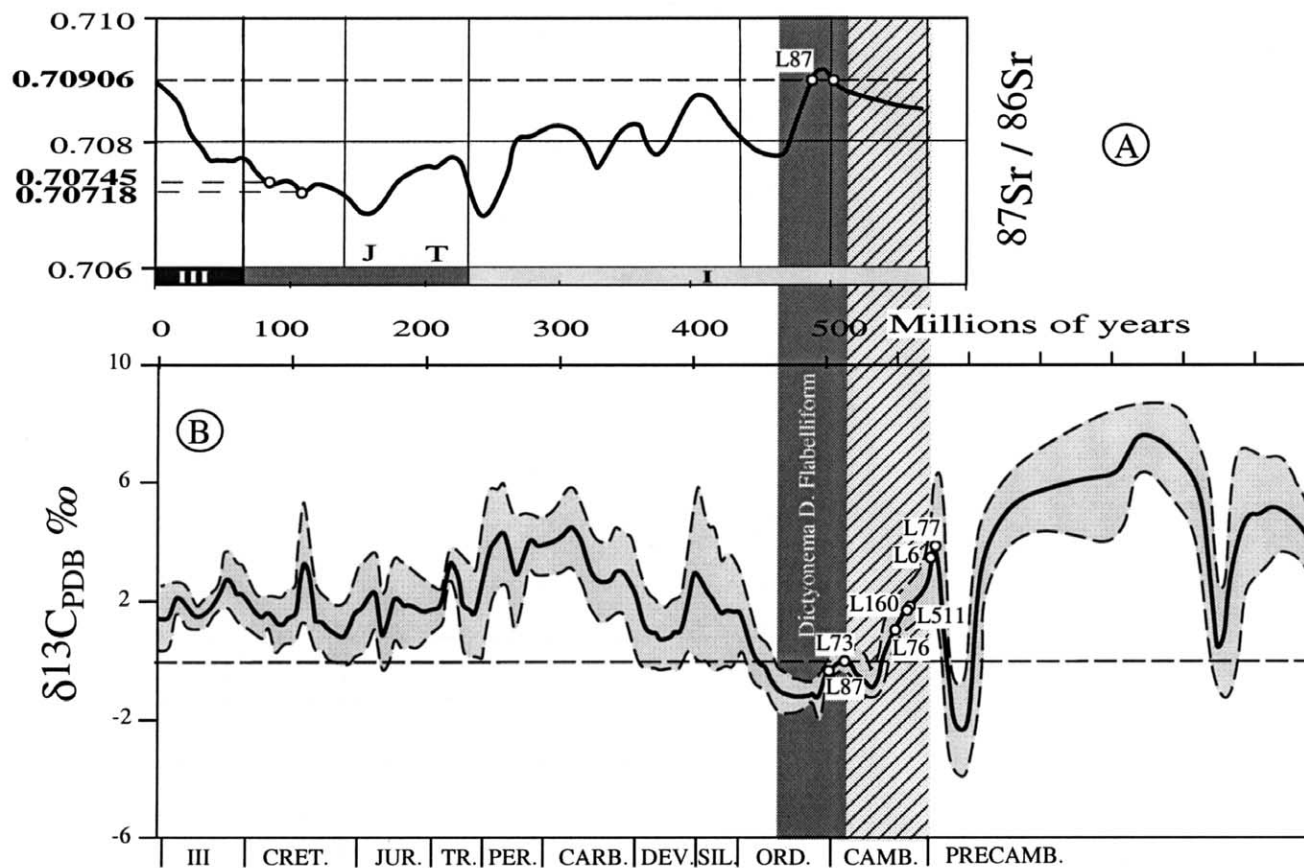
Fig. 7. A, $^{87}Sr/^{86}Sr$ values of analysed Karakoram and Ladakh marbles plotted on the Phanerozoic Sr isotope evolution curve of marine samples through time of Veizer al. [54]. B, $\delta^{13}C$ values of analysed Karakoram marbles, plotted on Phanerozoic $\delta^{13}C$ curve compiled by [54] (the shaded area corresponds to ± 1 σ gaussian distribution).

the Cambrian – Ordovician boundary. To test the validity of this Sr-age estimation, two foraminifera-bearing samples of known age (*Mesorbitolina*, Albian-Cenomanian), from the neighbouring Shyok Suture Zone, were analysed with the same method. Their $^{87}Sr/^{86}Sr$ ratios are concordant with the palaeontological age, confirming the validity of the geochronological method.

- A complementary method of ^{13}C dating has been used (Table II and Fig. 7b) to estimate ages of samples from the low grade zone of Upper Thalle valley to the high-grade zone of the Braldu valley. Upper Thalle samples (L76-L87) display low $\delta^{13}C_{PDB}$ values, which plot from the Cambrian-Ordovician transition to the Upper Cambrian on the curve compiled from [54,55]. Samples from the northern and western parts of the Lower Palaeozoic series (L6, L160 & L511) show higher $\delta^{13}C_{PDB}$ values, suggesting a Lower Cambrian age. All these are interpreted as sedimentary ages because any open system metamorphic effects would have shifted the $\delta^{13}C_{PDB}$ downwards [e.g., 56].

3.3. The Masherbrum Greenstone Complex

3.3.1. Structure

The Masherbrum Greenstone Complex is a kilometre thick sequence best preserved on the SW side of the Masherbrum glacier at elevations from 3900 to 6000 m (Figs 2 and 8). It mainly consists of discontinuous slices, generally about 100 m thick, of metagabbros, metavolcanics, ultramafic cumulates and metapelites, which may be interpreted as a dismembered ophiolitic sequence from field observations alone. The whole series defines a kilometre-thick unit folded inside the Dumordo marbles (Figs 8 and 9A–B). The curved shape of the tectonic slices of different origins, which appear to thin and truncate laterally show that initial tectonic stacking of units occurred before folding. The superposition of ophiolitic slices on serpentinised ultramafics shows that the serpentinite lithologies may behave as "soap-rock layers", and that the "décollement" was possibly initiated during an intra-oceanic stacking event. The whole sequence was subsequently thrusted over the Lower Palaeozoic marble series (Figs 8 and 9A–B). The
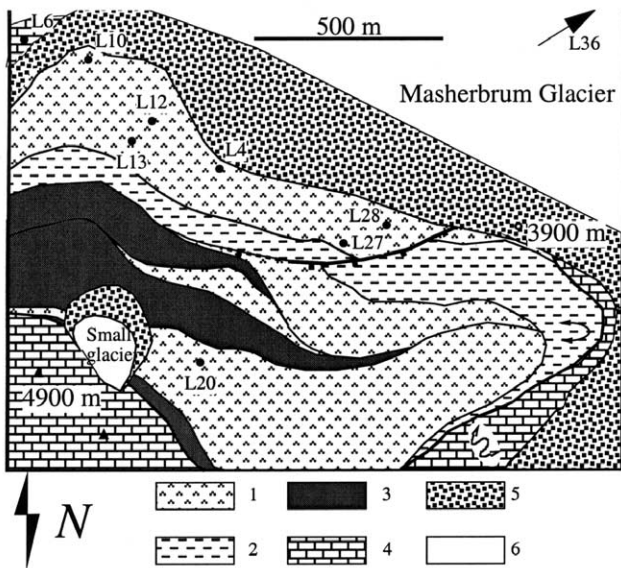
Fig. 8. Geological map of the Masherbrum Greenstone Complex. 1, gabbro-dioritic rocks; 2, volcano-sedimentary rocks; 3, ultramafic rocks; 4, crinoid-graptolite bearing marbles; 5, screens, torrential alluviums and moraines; 6, glacier.

directions of the south-vergent (dipping 40-80°N) folds and contacts range between 90 and 110°E, showing a strong transposition of all original tectonic and lithological surfaces in the direction of Eocene-Miocene Himalayan phase structures (as for instance the Shyok Suture Zone, 20 km to the south; Fig. 2). The Himalayan phase deformation was mainly ductile and characterised by large and steep isoclinal folds. Some south-dipping faults (φ in Fig. 9B), associated with ductile normal shearing reactivate the tectonic pile, probably as a consequence of Miocene Baltoro Batholith intrusion and doming, which occur to the north [6–8].

3.3.2. Lithology

The lower slices of the complex (200-300 m; a in Fig. 9B) are comprised of metagabbros cross-cut by a 10-40 cm thick doleritic dyke swarm. In thin section, both gabbros and dolerites show finely recrystallised pyroxene patches into acicular amphibole (< 1 mm long) and triple-jointed albite ± epidote grains.

A ~ 100 m thick slice of volcano-sedimentary formations is interlayered within the lower gabbroic sequence (b in Fig. 9B). These formations are made up of thin (0.5-30 cm) layers of metabasites and metapelites, and rare bands of leptynite. In thin section, the metapelites are finely recrystallised into muscovite – quartz – biotite – albite ± garnet ± staurolite, whereas the metabasites are finely recrystallised into tschermackite – albite – epidote ± biotite. The very thin structure of the rocks and layering can be interpreted as fine alternance of volcanic tuff and sediments.

Further up, irregular slices of altered and serpentinized meta-harzburgites (150-200 m thick; c in Fig. 9B) overlie the metagabbros. These ultramafic rocks are made up of thick talc - Mg-chlorite – magnesite layers, containing preserved boudin cores of serpentinite. Serpentinite is made up of minor amounts of calcite (5-15 mode%) together with antigorite and bastite (90-80 mode%) and millimetre-large rounded chrome spinel cores, surrounded by magnetite rims (1-8%). Serpentinite texture and mineralogy indicate greenschist-grade replacement of clinopyroxene, olivine and orthopyroxene. The protolith of these ultramafic rocks could have been of harzburgitic composition regarding minor proportion of calcite in replacement to clinopyroxene. Local presence of chrome spinel layers shows the cumulative nature of the ultramafic series.

At the top of the series (d in Fig. 9B), a thick band of dark metabasites is sandwiched between two layers of ultramafics. The rocks are very homogeneous, black and finely recrystallised. In thin sections, they show recrystallisation of mm-large calcite - chlorite - actinolite - albite crystals with no trace of previous phenocrysts, that could reflect aphanitic lava protolith.

Consequently, we interpret the lithological associations of the Masherbrum Greenstone Complex as dismembered sections of an ophiolite series defined as harzburgitic ophiolite type by Coleman and Nicolas [57,58]. From field investigations, the following reconstitution can be proposed, from base to top:

(1) the ultramafics present evidence of layering and segregation, and could represent the transitional zone or basal cumulative zone of an oceanic crust;
(2) the gabbroic section, cross-cut by the sheeted dyke swarm, could represent the cumulative ophiolitic section;
(3) the basaltic section at the sea-floor level forms the upper part of the ophiolite;
(4) the overlying pelagic / volcaniclastic sediments.

3.3.3. Mineralogy

The initial mineralogical assemblages such as the primary minerals pyroxene – plagioclase, recognisable texturally in the metabasites, recrystallised into albite - tschermakite - epidote ± biotite as a consequence of the Himalayan phase metamorphism. Metapelites with biotite - muscovite - albite - quartz ± garnet ± staurolite, define epidote-amphibolite facies metamorphic conditions.

Spinel grains have well-preserved chromitic cores (Table III and Fig. 10A), with high Cr_2O_3 (> 40 wt%), moderate Al_2O_3 (~ 20 wt%), FeO_t (~ 25 wt%), MgO (~ 5wt%) and TiO_2 (< 0.1 wt%) contents, although their rims are magnetite. In a plot of Cr# (atomic ratio of Cr/[Cr+Al]) vs. Mg# (atomic ratio of Mg/[Mg+Fe^{2+}]) for core compositions, Masherbrum spinels have Cr# and Mg# in the compositional field of volcanic arcs [59,60] (Fig. 10B), plotting in the field of Kohistan arc spinels [61]. Considering their low Fe# (atomic ratio of Fe/[Fe + Cr + Al]) and TiO_2, Masher
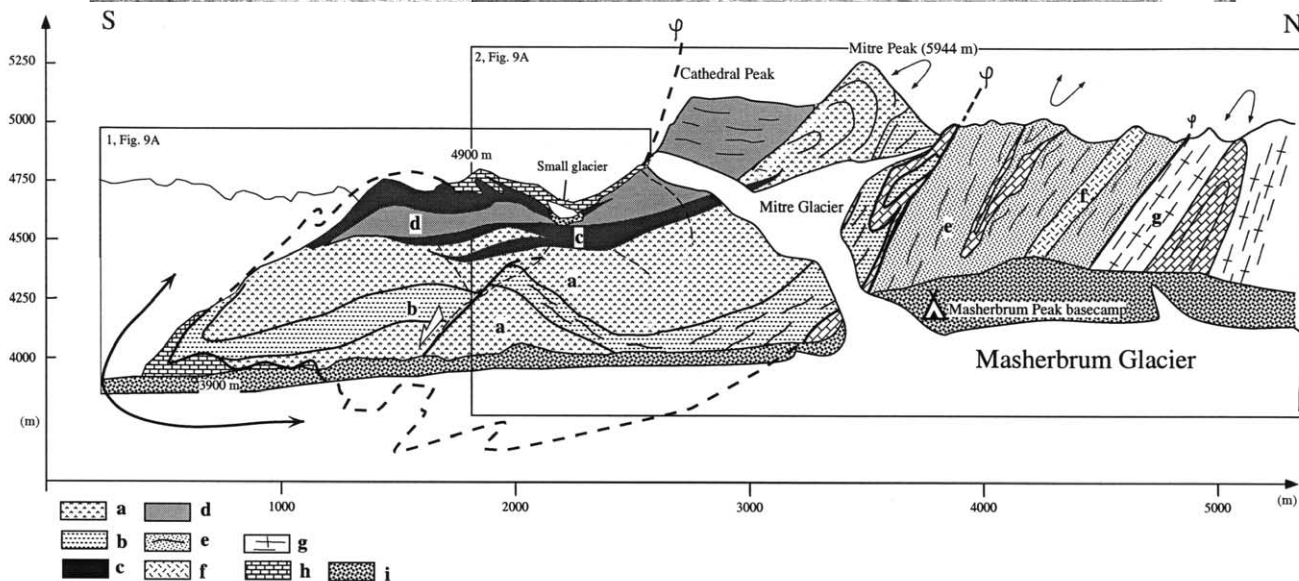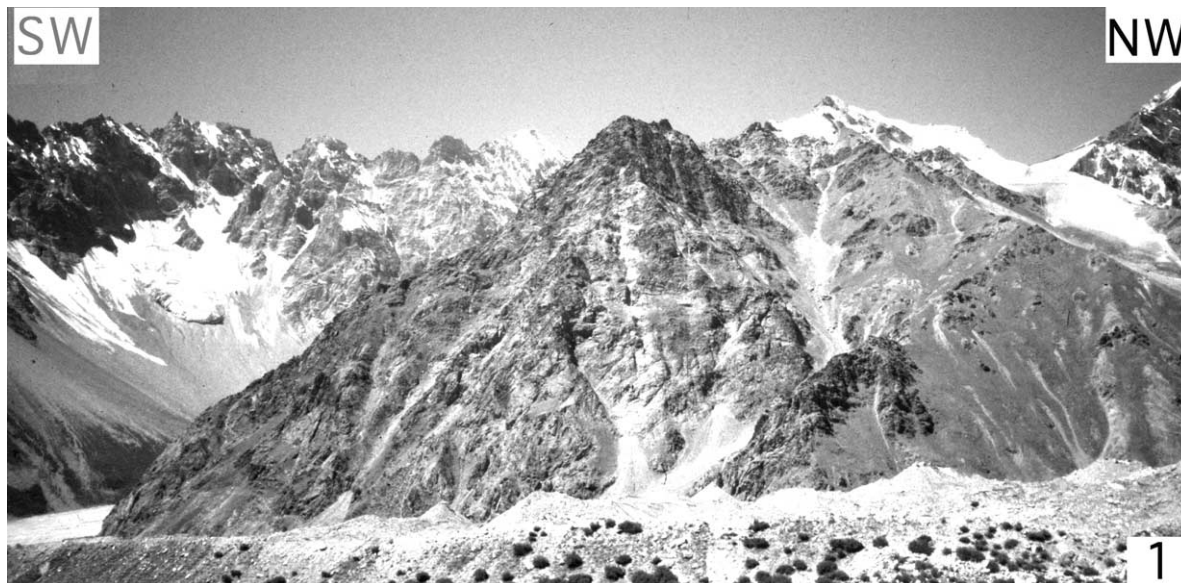
Fig. 9. A, panoramic view of the Masherbrum Greenstone Complex (the photographs were taken from the left side of the glacier). B, geological cross-section corresponding to photographs 1 and 2 of Fig. 9A. a, gabbroic slices; b, volcano-sedimentary slice; c, ultramafics; d, metabasaltic slice; e, metapelites (Ganshen Unit); f, granitic dyke; g, orthogneisses; h, marbles; i, moraines, screens and alluviums.

Table III
Representative compositionnal profile of a spinel grain (size: 2.5 mm), from the Masherbrum Greenstone Complex.

Mineral position	magnetite rim	M rim	M-C rim	M-C rim	chromite core	C core	C core	C core	C core	C core	chromite core	magnetite rim
SiO$_2$	0,11	0,00	0,93	0,00	0,03	0,01	0,00	0,34	0,04	0,00	0,00	0,27
MgO	0,17	0,73	1,77	1,12	4,42	5,28	5,43	4,13	5,51	4,95	1,60	0,79
Al$_2$O$_3$	0,01	0,69	0,67	3,24	20,56	20,75	20,67	17,62	20,55	20,23	6,33	1,69
TiO2	0,13	0,07	0,04	0,05	0,00	0,06	0,01	0,03	0,03	0,02	0,05	0,01
FeO	84,35	55,52	56,27	51,72	27,65	26,32	26,11	28,69	26,00	26,92	47,58	71,96
Cr$_2$O$_3$	1,88	36,52	33,04	37,12	42,14	43,05	43,42	39,67	44,15	43,39	38,91	19,13
MnO	0,21	1,35	1,46	1,30	0,91	0,79	0,79	0,78	0,95	0,98	1,35	0,55
FeO	28,49	29,11	27,25	28,82	27,01	25,93	25,71	25,76	25,65	26,25	28,90	29,92
Fe2O3	62,35	31,11	35,07	27,31	3,11	2,51	2,42	6,02	2,39	2,86	22,78	48,13
total	93,35	99,57	100,23	98,95	98,18	98,37	98,43	94,35	99,26	98,68	99,92	100,49
Calc. based on 32 O												
Si	0,04	0,00	0,28	0,00	0,01	0,00	0,00	0,10	0,01	0,00	0,00	0,08
Mg	0,08	0,33	0,79	0,50	1,76	2,08	2,14	1,74	2,16	1,96	0,69	0,35
Al	0,00	0,25	0,24	1,14	6,47	6,48	6,44	5,86	6,36	6,32	2,15	0,60
Ti	0,03	0,01	0,01	0,01	0,00	0,01	0,00	0,01	0,01	0,00	0,01	0,00
Fe^{2+}	7,84	6,15	6,05	5,94	4,62	4,52	4,51	4,71	4,49	4,56	5,67	6,87
Fe^{3+}	15,43	7,83	8,07	6,94	1,56	1,30	1,26	2,06	1,22	1,41	5,82	11,18
Cr	0,49	8,69	7,84	8,74	8,90	9,01	9,08	8,85	9,16	9,10	8,88	4,54
Mn	0,06	0,34	0,37	0,33	0,21	0,18	0,18	0,19	0,21	0,22	0,33	0,14
Cr#	0,99	0,97	0,97	0,88	0,58	0,58	0,58	0,60	0,59	0,59	0,80	0,88
Mg#	0,01	0,04	0,10	0,06	0,23	0,27	0,27	0,22	0,28	0,25	0,09	0,04

brum spinels appear to be very close to boninitic mantle spinels [62] (Fig. 10C). Consequently, spinel mineralogy reflects a volcanic arc setting rather than an oceanic crust setting.

3.3.4. Geochemistry

Eight samples have been collected through the different mafic and ultramafic slices of the Masherbrum Greenstone Complex (cf. Fig. 8) and analysed by XRF and ICP-MS for major and trace elements (see analytical method in annex and Table I). Major element data, featured by Harker plots on Fig. 11, are characterised by relatively high Al$_2$O$_3$ and CaO, and low TiO$_2$ and Na$_2$O+K$_2$O contents, featuring tholeiitic arc to calc-alkaline arc lava compositions. Three samples are different. Metabasalt L20 has higher FeO$_t$, TiO$_2$ and lower Al$_2$O$_3$ than the rest of the series at equivalent MgO or SiO$_2$ contents. The particularly high TiO$_2$ and low Al$_2$O$_3$ contents of L20 are typical of OIB lavas, though Na$_2$O and K$_2$O are low. Dolerite L13 shows elevated MgO and SiO$_2$ contents of are characteristic of high-Mg andesitic compositions. For L27, the lower Al$_2$O$_3$ content is associated with lower CaO and higher Na$_2$O contents, which could be due to anorthite-rich plagioclase removal at relatively high silica content (60 wt%).

Trace element data allow more distinctions between these rocks. Although recent studies have reached different conclusions concerning trace element mobility due to fluid metasomatism, there is however a general consensus for considering LILE, Cs, U, and P mobile and Th, Ta, Nb and REE, relatively immobile in aqueous fluids [67–69]. On the basis of these less mobile elements, the calc-alkaline to tholeiitic samples can be separated into two types (Fig. 12):

- (i) type 1 (samples L4, L10, L12) is characterised by enrichments in LREE (Light Rare Earth Elements) vs. HREE (Heavy Rare Earth Elements), with relatively high (La/Sm)$_N$ and (La/Yb)$_N$ (Table I). MORB-normalised spidergrams (Fig. 12A) show clear negative Nb-Ta and Ti anomalies and positive Th anomalies, characteristic of an arc setting [70,71].
- (ii) type 2 (samples L27, L28, L36) is featured by depleted to flat LREE patterns, showing very slight negative Nb-Ta, and positive Th anomalies (Fig. 12B). These features are intermediate between MORB and arc settings, which is often interpreted to represent a back-arc basin environment [72–74].

Some fractional crystallisation of Ti-oxides and plagioclase are suggested by negative Ti and Eu anomalies in Fig. 12 spidergrams, for both types.

Samples L20 and L13 show contrasting REE and trace elements patterns (Fig. 12C). L13 high-Mg dolerite shows slight arc features, with only slight Nb-Ta and strong P and moderate Ti negative anomalies, a marked Th positive anomaly. This sample has LREE enrichment (similar to type 1 lavas) and a flat HREE pattern, features currently observed in high-Mg andesites (e.g., Shinjo [49]). L20 metabasalt displays a very strong LREE enrichment and HREE depletion, but no Nb-Ta negative anomaly, which is typical of alkali and more likely OIB-type lavas except a marked depletion in LILE. This depletion in LILE and the low values of K$_2$O and Na$_2$O are not coherent regarding the very
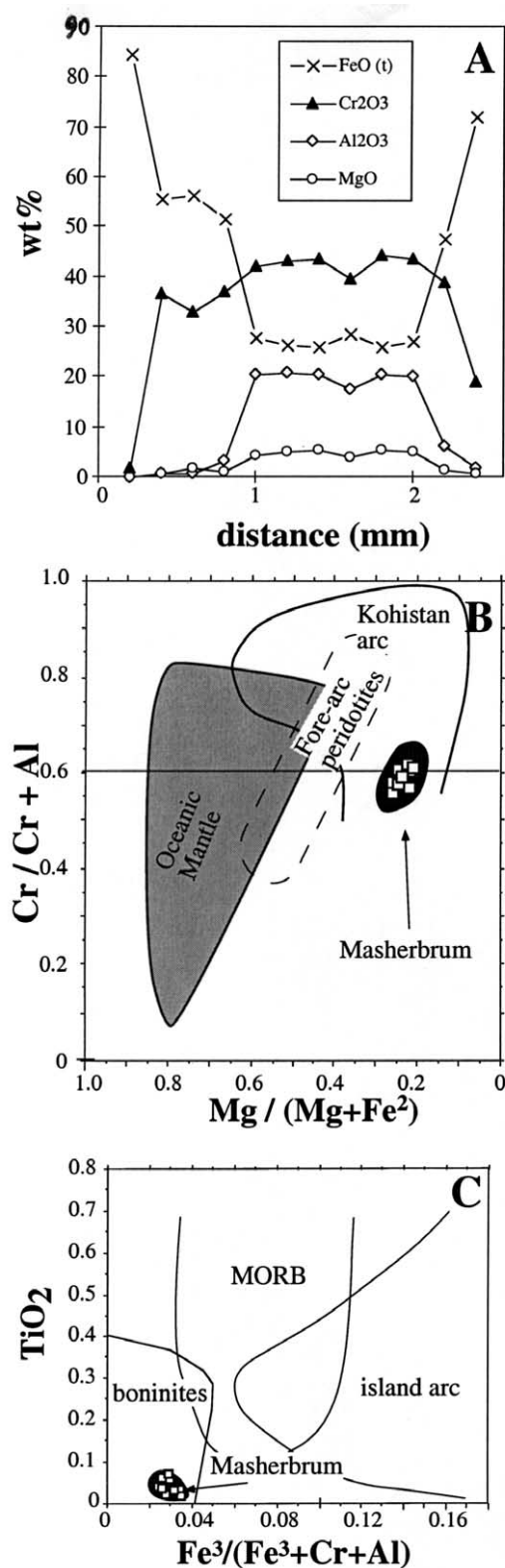
Fig. 10. Chemical composition of Masherbrum Cr-spinels. A, single-mineral profiles. B, Cr# vs. Mg# diagram; the field for oceanic mantle is from Dick and Bullen [63], the field for fore-arc mantle is from Parkinson and Pearce [64] and Ishii et al. [65] and the field of Kohistan arc complex mantle is from Jan and Windley [61]. C, TiO_2 vs. Fe# diagram from Orberger et al. [62]. Only spinel core values are plotted in B and C diagrams.
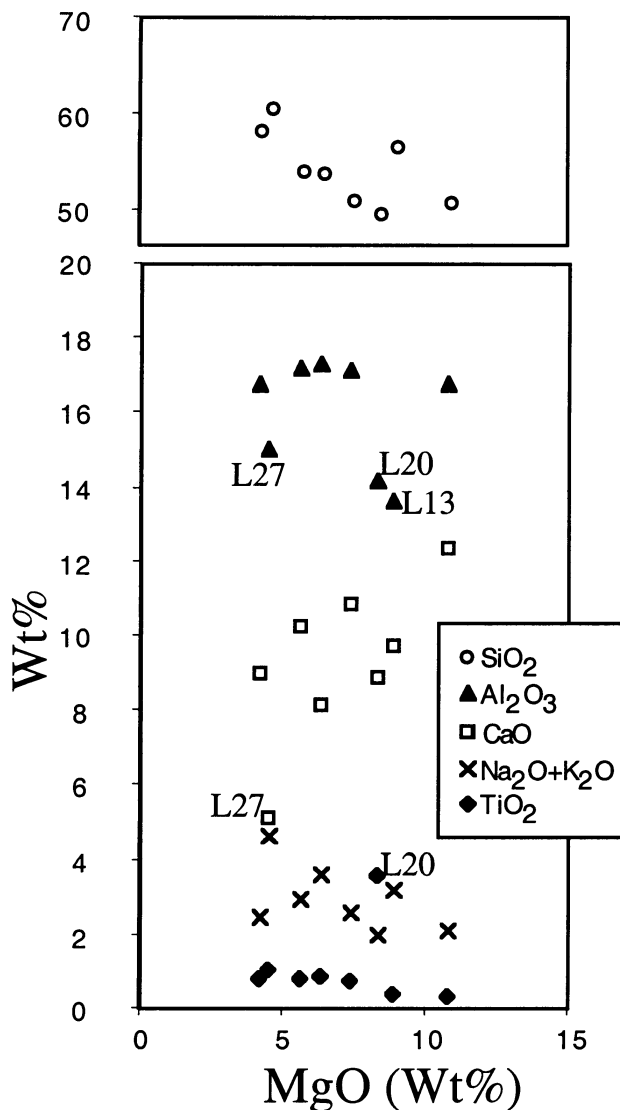

Fig. 11. Harker plots of Masherbrum magmatic rocks.

high Th and LREE values of this metabasalt, so we propose that they are more likely due to alteration/metamorphic effects, which are probably very sensitive for this lava with such a high LOI of 8.9 wt%.

As the importance of the Nb-Ta depletions are generally diagnostic of supra-subductive settings and Th enrichments of contamination by a crustal component, a Ta/Yb vs. Th/Yb diagram has been used to evaluate the arc affinity and crustal components in geochemical signatures (Pearce [75]; Fig. 13). Hence, in order to compare the Masherbrum rocks with current arc – back-arc settings, we have also plotted the values of Vanuatu and Mariana arc lavas and of North Fiji basin dragged samples [76–78]. The Masherbrum arc-type samples (L4, L10 and L12) have high Th/Yb and low to intermediate Ta/Yb ratios, at the transition between calc-alkaline lavas and shoshonitic lavas [75]. They show similar Th/Yb ratios as most differentiated Vanuatu arc lavas, but
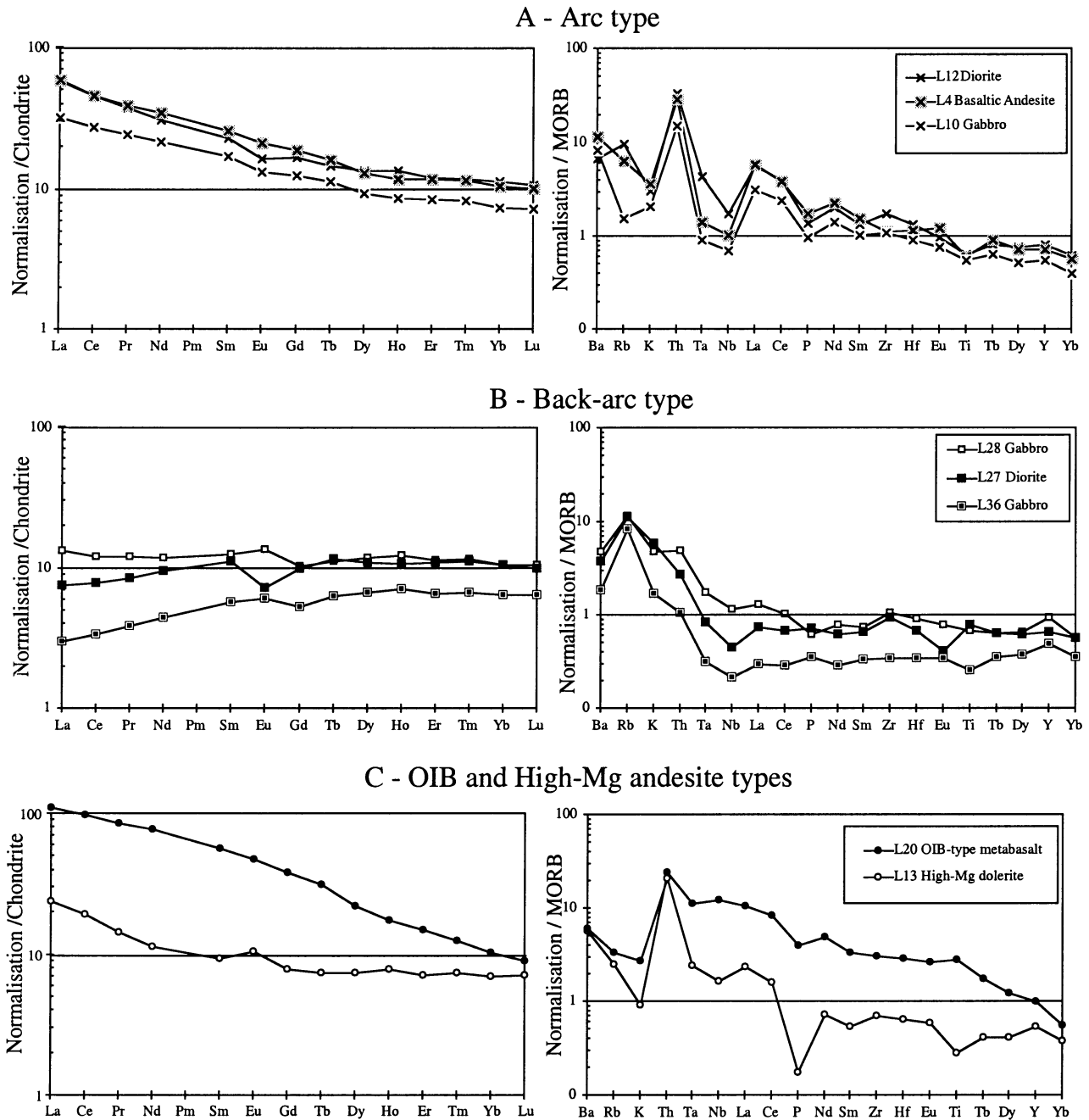
Fig. 12. A, Chondrite-normalised and B, MORB-normalised element patterns of Masherbrum Greenstone Complex magmatic rocks. Chondrite normalisation values are from Evensen et al. [66] and MORB normalisation values are from Sun & Mac Donough [47].

transitional Ta/Yb ratios, between most differentiated Vanuatu arc lavas and OIBs.

The depleted-undepleted LREE samples (L27, L28, L36) show lower Ta/Yb and Th/Yb values, similar to tholeiitic arc series [75]. These samples plot between the fields of N-MORBs and those of primitive Mariana and Vanuatu arc lavas, with some Th enrichment probably linked to a subduction dehydration fluid component (S in Fig. 13, [75]). The shift towards higher Ta/Yb and Th/Yb for sample L28

features enrichment in both Nb-Ta and Th, that may be due to the source (W in Fig. 13). Back-arc basin lavas are generally distinguished from MORBs considering their relative LREE, LILE (Large Ion Lithophile Elements) and Th enrichments and Nb-Ta negative anomalies, linked to the influence of subduction [e.g., 71]. Considering that the LREE-depleted / flat patterned samples show intermediate geochemical features between MORB and arc lavas, they more likely represent a back-arc basin environment.
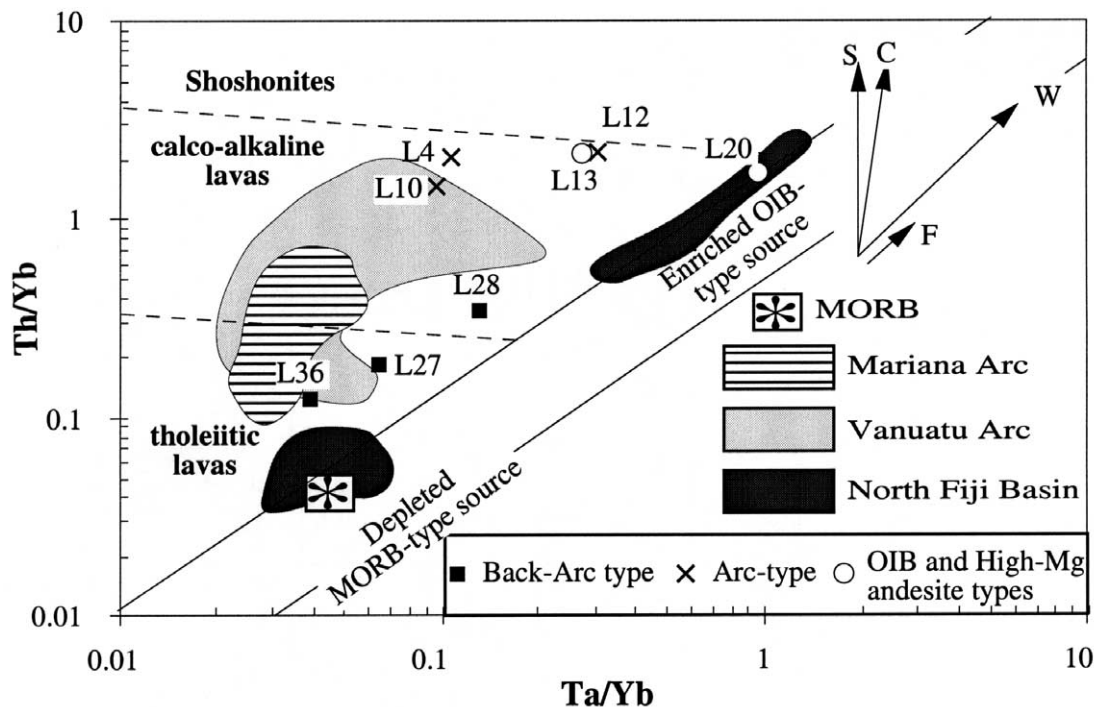
Fig. 13. Ta/Yb vs. Th/Yb diagram of Pearce [75]. The vectors indicate geochemical variations linked to: crystal fractionation (F), source effects (W), crustal contamination (C) and subduction metasomatism (S).

The two particular samples show higher Ta/Yb ratios. Dolerite L13 plot in the upper calc-alkaline field, with transitional Ta/Yb ratio between OIB and most differentiated Vanuatu arc lavas. The alkaline metabasalt L20 show Ta/Yb ratio in the field of OIB-type lavas.

In summary, the Masherbrum Greenstone Complex preserves contrasting geochemical types: a LREE-enriched type similar to lavas erupted in current evolved arc settings, a LREE-depleted type similar to the lavas emplaced in back-arc settings, and two particular lavas suggesting the contribution of OIB and/or pelagic sediments sources. These contrasting geochemical types, which are interlayered, suggest either the aggregation of different blocks or heterogeneities in the source region. Answering this question requires an isotopic analyse of the samples.

3.3.5. Isotopic age of Masherbrum Greenstone Complex samples

The Masherbrum Greenstone Complex is folded inside Dumordo-like crinoid and graptolite bearing marbles of proposed Lower Ordovician to Cambrian age (see section 3.2). In order to check that the isotopic composition of the lavas is consistent with Lower Palaeozoic age, we have plotted $^{147}Sm/^{144}Nd$ vs. $^{143}Nd/^{144}Nd$ ratios on Fig. 14 (see analytical procedures in annex and Table I). The plot does not strictly define an isochron, as the rocks are not necessarily derived from the same source and may not be exactly contemporaneous. As samples L13 and L20 show distinct major, trace and isotopic characteristics, the right down-

going trend towards lower $^{143}Nd/^{144}Nd$ and higher $^{147}Sm/^{144}Nd$ (A in Fig. 14) may reflect the effect of the source, so these samples must be excluded for any age estimation of the MGC. However, using all the arc and back-arc type samples, an isochron age of 565 ± 272 (2σ) Ma can be calculated. In spite of the large error, these data are consistent with the proposed Lower Cambrian ^{13}C age of L6 carbonate (located on the lower part of the klippe, see Fig. 8) and exclude the Mesozoic age proposed by Searle [11] for these rocks.

3.3.6. Isotopic constraints on the nature of sources

The Sr isotope ratios may have been affected by alteration and metamorphism. For instance, $^{87}Sr/^{86}Sr$ ratios (Table I) define a wider range than $^{143}Nd/^{144}Nd$ ratios (e.g., L28 with both high εNd of 7.4 and very high εSr of 29.4); although high $^{87}Sr/^{86}Sr$ ratio can sometimes be correlated with low $^{143}Nd/^{144}Nd$ (e.g., L13). Discrimination between alteration/metamorphic effects and source effects does not seem possible on the basis of Sr isotopes alone. Nd isotopic ratios have been shown to be unaffected in low metamorphic grade terrains [67–69], and moreover were shown to be immobile in the neighbouring Shyok Suture Zone [79]. Thus, to evaluate the nature of the different sources, we have used an εNd$_{565}$ vs. Nb/La diagram (Fig. 15). The Nb/La ratio features the importance of Nb-Ta negative anomaly that is representative of the arc affinity of the lavas, while the εNd$_{565}$ ratio represents the enrichment level of the source. Values of Indian MORB mantle (IMM), of enriched
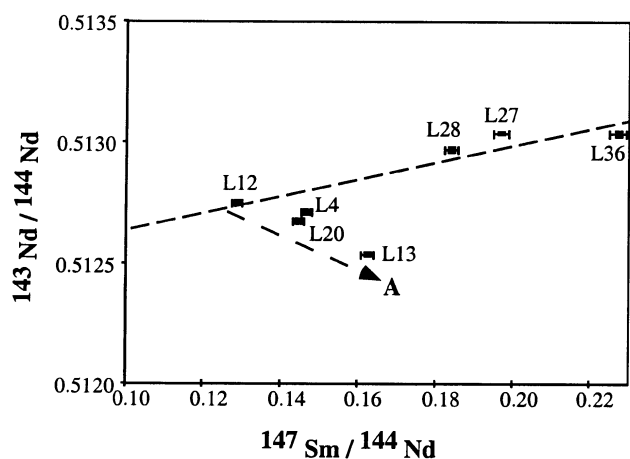
Fig. 14. ^{143}Nd /^{144}Nd vs. ^{147}Sm/^{144}Nd diagram. A trend towards lower Sm/Nd and ^{143}Nd /^{144}Nd ratios reflects source heterogeneity. Taking into account all arc and back-arc type samples (excluding L20 and L13), an age of 565 ± 272 Ma (Nd_i = 0.512976) can be calculated. This Lower Paleozoic age is in accordance with the Cambrian $\delta^{13}C$ age of marble L6 and other age results.

Fig. 15. εNd_{565} vs. $(Nb/La)_N$ diagram. The arc / back-arc type samples plot within arc compositional field [83], closer to IMM pole in the case of back-arc samples. The high-Mg dolerite plots close to the field of pelagic sediments, with a very low εNd (0.5), suggesting interactions between sediment melts and mantle [49]. L20 metabasalt yields also a low εNd, compatible with the contribution of an enriched OIB-type source.

mantle (EMII), OIB [80,81] and pelagic sediments [82] represent possible source components involved in magma genesis. The data mainly plot in the field defined for arc lavas by [83]. Samples L4 and L12 have very low Nb/La ratio and relatively high εNd_{565}, which are consistent with melting of a fluid-metasomatised arc mantle source (e.g., [84]). Samples L36, L28 and L27 have εNd_{565} and Nb/La ratios which are intermediate between arc-type lavas and IMM component, and imply a contribution of source material similar to IMM with minor fluid-metasomatic input. The high-Mg dolerite plots close to the field of pelagic sediments, with much lower εNd_{565} (0.54). This value is consistent with an increased contribution of an enriched source similar to pelagic sediments or EMII. Finally, sample L20 shows lower εNd_{565} (4.52) than arc and back-arc type samples and high Nb/La ratios, compatible with the contribution of an OIB-type component (e.g., [80]) or to mantle-adakitic melt interaction [52,79].

4. Discussion

A wide variety of geological formations are observed within the low grade metamorphic zone of the south-eastern Karakoram margin. The section from the southern limb of Karakoram to the Baltoro Batholith reveals a Precambrian basement, exposed north of the Shyok Suture Zone, overlaid by a thick pile of Cambro-Ordovician platform-type sediments, deposited in a detrital environment. These southern Karakoram series were thrusted over by a complex ophiolitic series, the Masherbrum Complex, which witnessed the intra-oceanic accretion of various arc, back-arc and possibly OIB, slices, representative of the geodynamics of the Karakoram in the Cambro-Ordovician period. These results can be compared with other parts of Karakoram in order to
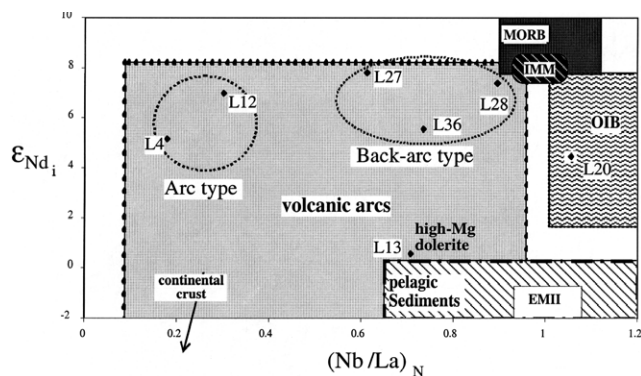
test the lateral continuity of the Karakoram block, and discussed about the geodynamics of central-eastern Asia in Lower Palaeozoic times.

4.1. Longitudinal continuity and geology of the Southern Karakoram margin

The northern Karakoram has been shown to be a continuous belt of Upper Palaeozoic to Middle Mesozoic series from the north-western Karakoram and Hindu Kush to the west, and to the Upper Hunza valley in the east [20,22]. The discovery of a Precambrian basement overlain by Cambro-Ordovician series in south-eastern Karakoram provides evidence of geological longitudinal continuity within the ~ 500 km long Southern Karakoram margin (Fig. 1), as in the northern part of Karakoram. The south-eastern Karakoram series described in this paper appear to be quite similar to those described in south-western Karakoram in the area of Chitral [2]. At the base of the south-western Karakoram sedimentary pile, the Yarkun Formation is a thick sequence of terrigenous sediments, mainly quartz-arenites in the lower half, becoming more calcareous at the top, resembling the Ganshen and Dumordo units. Both in western and eastern Karakoram, these Cambro-Ordovician series overlie older basements, Precambrian in the east and probably Cambrian (ante-Arenigian) in the west. The Precambrian basement of eastern Karakoram itself was formed in a context of subduction and arc magmatism and probably under high-temperature conditions, as shown by the close geochemical affinity of Upper Thalle Precambrian basement with adakites and Archean tonalites-trondhjemites-granodiorites (e.g., [53]). But the basement described in western Karakoram is more alkaline and probably younger [2]. Thus the Karakoram basement is not laterally homogeneous neither in composition nor in age. However, these

Precambrian rocks were eroded before the sedimentation of the Cambro-Ordovician series.

The longitudinal coherence of the Karakoram block ends at the contact with the Karakoram Fault [85]. On the eastern side of the Karakoram Fault, similar successions of Cambro-Ordovician series overlying an older crystalline basement as those of the south Karakoram, are only found in the Lhasa block, where an Early Cambrian basement gneiss (539 ± 14 Ma, [86]) is overlain by unmetamorphosed Ordovician sediments [87]. Both the Lhasa and Karakoram blocks were accreted in the Lower Cretaceous times [88–90]. If Lhasa and Karakoram blocks were initially the same geological block, the offset of the Karakoram Fault would be ~ 300 km, based on the current positions of the Kilik fault (northern boundary of Karakoram, [4,29]) and of the Bangong suture (northern boundary of the Lhasa block; Fig. 1).

4.2. Lower Palaeozoic Arc dynamics at the limb of central-eastern asian blocks

Previous studies in Central-Eastern Asia have shown that this region is made of blocks and terranes that were accreted from the Lower Palaeozoic to the Tertiary. Cambro-Ordovician ophiolites, in most cases presenting volcanic arc affinities, have been described in most sutures of central-eastern Asia: in the south Tianshan of the Pamirs [91]; in the northern Kunlun - southern Tarim ophiolitic belt [92,93]; in the northern Tarim-Yili-Junggar ophiolitic belt [94,95]; and in the suture between north and south China Blocks [96]. Consequently, arc magmatism appears to be a common feature of Cambro-Ordovician central-eastern Asia suture zones.

The samples studied in SE Karakoram show contrasted geochemical types. Although the Masherbrum Complex displays an ophiolitic association, suggestive of an oceanic crust section in the field, the chemistry of chrome spinels and the geochemistry of most gabbroic and basaltic rocks which are interlayered in the series indicate that the Masherbrum Complex is a tectonic sequence of various origins which were thrusted on each other (Fig. 16). These differences can be interpreted in terms of different geodynamic settings: arc, back-arc and OIB. Similar Cambro-Ordovician associations of arc and OIB-type lavas has been observed in South Tianshan [91]. However, such geochemical features as those of the OIB-type lava (sample L20) have been found in current arc settings [52], so we are not able to discriminate between OIB and arc settings on the basis of only one sample. Furthermore, the presence of an high-Mg andesitic dolerite (sample L13) in the arc series with a very low εNd ratio, can also be interpreted as resulting from mantle-adakitic melt interactions [49], so that the presence of Nb-rich magmatism (sample L20) within the arc series is plausible.

4.3. Geodynamic significance of the Masherbrum Greenstone Complex

The stacking of the different tectonic slices separated by thick bands of ultramafics, favours the hypothesis of intra-oceanic piling processes, possibly in consequence to the closure of the back-arc domain (Fig. 16B). A similar interpretation has been proposed for the neighbouring Shyok Suture Zone (30 km to the south) in Upper Cretaceous times [34,97]. The geochemical and structural likeness of the Shyok Suture Zone shows the recurrence of similar back-arc and arc accretion dynamics on long-time span intervals (~ 400 Ma) in the same zone. Such superpositions of contrasted geochemical types of ophiolites, separated by irregular contacts underlined by serpentinised ultramafics, overthrusted over carbonate platforms are also reported in the Greek Hellenides, where they are thought to result from intra-oceanic subduction [98]. The obduction of the ophiolite over sedimentary platform could have preceded the collision of two blocks (southern and northern blocks) within the Karakoram (Fig. 16B).

5. Conclusions

Despite deformation and metamorphism that affected most of the south central Karakoram during Himalayan orogeny, the less metamorphosed south-eastern Karakoram formations preserve Cambro-Ordovician platform-type series, uncomformably resting on a basement displaying a minimum age of 651 Ma. The Lower Palaeozoic sedimentary series appear to be similar to those occurring in south-western Karakoram, which show that the Karakoram is a continuous tectonic block. Coupled relative (palaeontological), and isotopic ($^{87}Sr/^{86}Sr$ and ^{13}C) datings have shown that the age of the carbonates ranges from Lower Cambrian to Lower Ordovician.

The Cambro-Ordovician series display a relic pile of ophiolitic rocks (the Masherbrum Greenstone Complex) which has witnessed the geodynamic evolution of the Karakoram in the Cambro-Ordovician. The Masherbrum Greenstone Complex shows the stacking of several slices of magmatic rocks with lithological features interpretable from field observations as an obducted oceanic crust sequence. However, the mineral chemistry of ultramafic rocks and geochemistry of magmatic rocks evidences the occurrence of different parts of an arc – back-arc system. Isotope geochemistry shows that back-arc and arc rocks are derived from depleted and slightly enriched mantle sources, respectively. Two samples (L13 and L20) feature more important contribution of an enriched mantle source. Along with slight arc characteristics considering REE and trace elements, high-Mg dolerite L13 features mantle source heterogeneity in the source region of the arc, and possibly increased contribution of pelagic sediments. High εNd and Nb/La
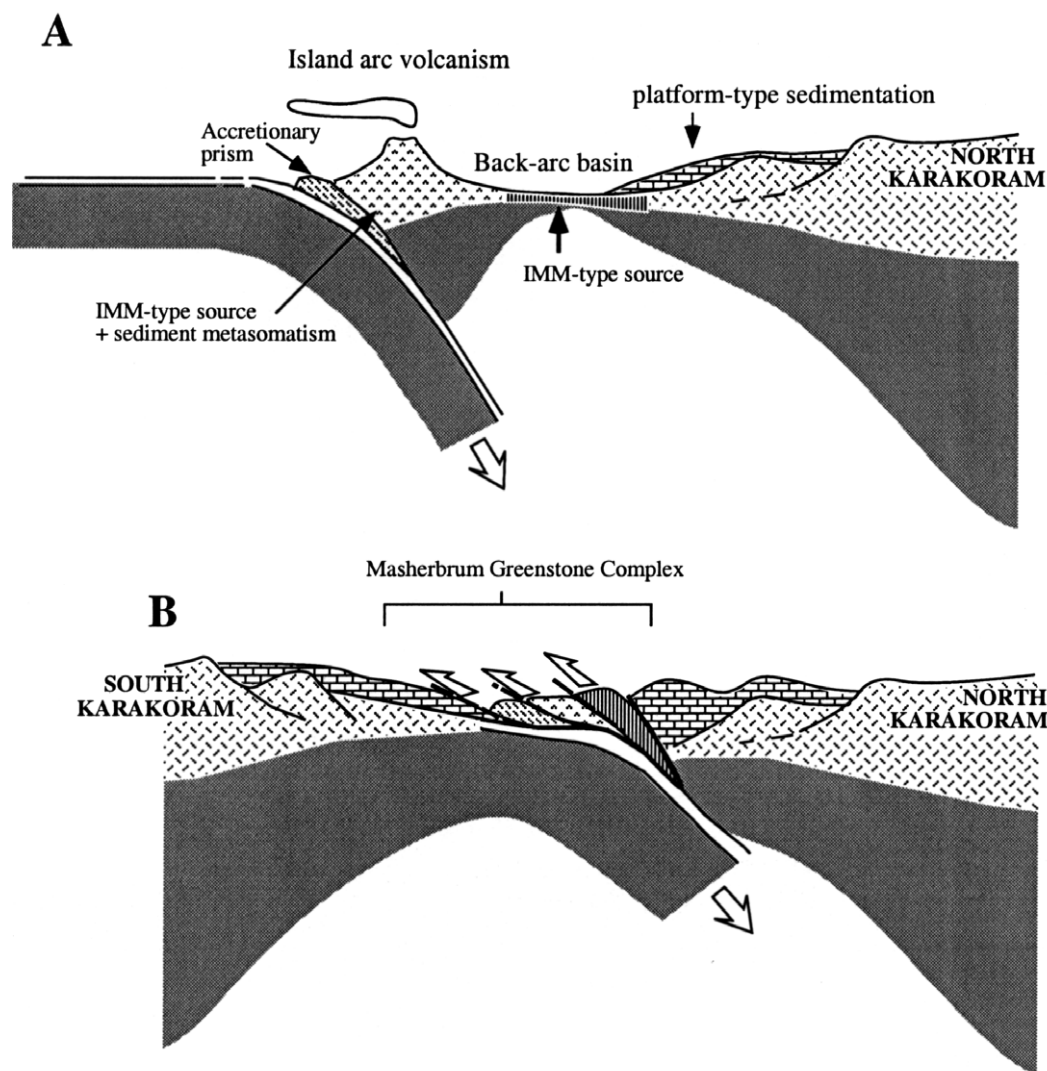
Fig. 16. Schematic diagram illustrating the tectonic evolution proposed for the Karakoram in Lower Ordovician times. A, during the Lower Ordovician period, a phase of subduction has occurred, characterised by the formation of volcanic arc and back-arc series along the southern margin of a Northern Karakoram continental micro-block. Arc series were formed by melting of an IMM-type source by sediment-dehydration and melting metasomatism, while back-arc series were formed by melting of a nearly pure IMM-type source. B, intra-oceanic accretionary phase of the arc system and closure of the back-arc domain. The arc and back-arc tectonic pile was afterwards obducted over the sedimentary platform (Lower Palaeozoic series) of the southern Karakoram block.

ratios of metabasalt L20, could represent either Ocean Island stacking or Nb-rich arc magmatism.

Consequently, the Masherbrum complex is another example of Cambro-Ordovician arc ophiolite, showing that arc dynamics were omnipresent at the limb of most central-eastern Asian micro-blocks during the Cambro-Ordovician. This result is consistent with palaeomagnetic studies in central-eastern Asia, which have shown that central-eastern Asian was a puzzling tectonic network of micro-blocks, along with Siberia, Baltica, North China Block and North America that were not connected to the Gondwanaland but highly mobile during that period [99–102]. The complexity, polyphased and sometimes antithetic characters of some suture zones show that the most acceptable model concerning the tectonic situation of central-eastern Asia during the

Cambro-Ordovician period is that of a complex network of convergent and divergent blocks, close to the geodynamic situation of the current SW Pacific margin.

Acknowledgements

. Appendix: Analytical procedures

Mineral analyses were obtained on a Cameca SX-100 microprobe at the University Blaise Pascal of Clermont-Ferrand. Counting time was 10 sec. per element, the accelerating potential was 20 kV for a sample current of 20 nA. Natural silicates were used as standards.

Nine igneous rocks were analysed for major and trace elements (Table I). Major elements, Ni, Cr and Co were analysed using X-Ray fluorescence (XRF) at the University C. Bernard of Lyon. Loss on ignition (LOI) was determined by heating the sample at 1000°C for 30 minutes. For trace element analyse, samples were prepared and analysed following the method of Barrat et al. [103], using Inductively Coupled Plasma Mass Spectrometry (ICPMS) at the University J. Fourier of Grenoble. Reproducibility (at 2σ), based on 9 measurements of BHVO standard, is between 0.01 and 1 % for the Rare Earth Elements (REE) and between 0.01 and 6 % for all the other trace elements.

Seven igneous rocks (presented in Table I) and 3 marbles have also been analysed for their radiogenic isotopic composition, for sample preparation see [104]. Samples were leached twice in a 2N HCl - 0.1N HF mixture. For the determination of the $^{147}Sm/^{144}Nd$ ratio, samples were spiked with a solution of known $^{146}Nd/^{144}Nd$ composition. Sm, Nd and Sr isotopic compositions were determined on a Finnigan MAT 261 multicollector mass spectrometer at the University Paul Sabatier of Toulouse. Correction of the mass discrimination effect was made by normalising $^{143}Nd/^{144}Nd$ to a value of $^{146}Nd/^{144}Nd$ of 0.71219 and $^{87}Sr/^{86}Sr$ to a value of $^{88}Sr/^{86}Sr$ of 8.3752. Errors on the measurements on the $^{147}Sm/^{144}Nd$ ratio are of 1% (2σ). Eight marble samples were also selected for stable isotope analysis (for analytical procedures, see [105]). $\delta^{13}C_{PDB}$ analysis of NBS18 standard yielded –5.01. Analytical precision (extraction + spectrometer) was ± 0.05 per mil.

Sample L131, selected for Amphibole Ar-Ar dating was irradiated at the TRIGA reactor in Pavia, and analysed at the isotope geology laboratory of Bern University. The sample was heated in a double vacuum resistance furnace. Ar was analysed in a MAP 215-50B rare gas spectrometer. The Ar-Ar results are presented in Fig. 5, for more details about analytical procedures see [45].

References

[1] J.A. Talent, R. Mawson, Palaeozoic-Mesozoic biostratigraphy of Pakistan in relation to biogeography and the coaelescence of Asia, in: A. Farah, K.A. Dejong (Eds.), Geodynamics of Pakistan, Quetta Geological Survey of Pakistan, 1979, pp. 81–102.

[2] P. Le Fort, M. Tongiorgi, M. Gaetani, Discovery of a crystalline basement and Early Ordovician marine transgression in the Karakorum mountain range, Pakistan, Geology 22 (1994) 941–944.

[3] M. Gaetani, P. Le Fort, S. Tanoli, L. Angiolini, A. Nicora, D. Sciunnach, A. Khan, Reconnaissance geology in Upper Chitral, Baroghil and Karambar districts (northern Karakorum, Pakistan), Geol. Rundsch. 85 (1996) 683–704.

[4] M. Gaetani, E. Garzanti, F. Jadoul, A. Nicora, A. Tintori, M. Pasini, K.S. Ali Khan, The north Karakorum side of the Central Asia geopuzzle, Geol. Soc. Amer. 102 (1990a) 54–62.

[5] H.W. Flügel, M. Gaetani, Permian Rugosa from Northern Karakorum and Aghil Ranges, Riv. It. Paleont. Strat. 97 (1991) 35–48.

[6] J.M. Bertrand, J.R. Kienast, J.L. Pinardon, Structure and metamorphism of the Karakorum gneisses in the Braldu-Baltoro Valley (North Pakistan), Geodinamica Acta 2 (1988) 135–150.

[7] M.P. Searle, A.J. Rex, R. Tirrul, D.C. Rex, A. Barnicoat, B.F. Windley, Metamorphic, magmatic and tectonic evolution of the central Karakoram in the Biafo-Baltoro-Hushe regions of northern Pakistan, Geol. Soc. Amer. Spec. Pap. 232 (1989) 47–74.

[8] T. Allen, C.P. Chamberlain, Metamorphic evidence for an inverted crustal section, with constraints on the Main Karakorum Thrust, Baltistan, northern Pakistan, Journal of Metamorphic Geology 9 (1991) 403–418.

[9] Y. Lemennicier, P. Le Fort, B. Lombardo, A. Pêcher, F. Rolfo, Tectonometamorphic evolution of the central Karakorum (Baltistan - northern Pakistan), Tectonophysics 260 (1996) 119–143.

[10] Y. Rolland, G. Maheo, S. Guillot, A. Pêcher, Tectono-metamorphic evolution of the Karakoram Metamorphic complex (Dassu – Askole area, NE Pakistan): exhumation of a mid-crustal granulites in a convergent context, Journal of Metamorphic Geology 19 (2001) 717–737.

[11] M.P. Searle, Geology and Tectonics of the Karakorum Mountains, John Wiley and Sons, Chichester, 1991, pp. 358.

[12] A.M. Ver chère, Kashmir, the Western Himalaya and the Afghan Mountains, a Geological paper, Journal of Asiatic Society of Bengala 34 (II) (1867) 47–50.

[13] E. De Verneuil, Note on the fossils forwarded by Mr. Verchère, Appendix. Journal of Asiatic Society of Bengala 34 (II) (1867) 208–208.

[14] R. Lydekker, The Geology of the Kashmir and Chamba Territories, and the British district of Hhagan, Mem. Geol. Surv. India 22 (1883) 1–344.

[15] W. Campbell Smith, Notes on the rock-specimens collected by the Bullock Workman Expedition, 1911–1912 in the Bilaphon and Kondus Basins, and on the Khondokoro and Masherbrum glaciers, in: F. Bullock Workman, W.H. Workman (Eds.), "Two summers in the Ice-Wilds of Eastern Karakoram", Appendix, Fisher Unwin, London, 1917.

[16] G. Dainelli, Relazioni scientifiche della Spedizione Italiana "De Filippi" nell'Himàlaya Caracorùm e Turchestàn Cinese (1913–1914) Serie 2a, Risultati Geologici e Geografici, Vol. II, La serie dei Terreni, Zanichelli, Bologna, 1934.

[17] T.E. Gattinger, Geologischer Querschnitt des Karakorum vom Indus zum Shaksgam, Jahrb. Geol. Bundesanstalt, Sonderb., 6, Wien, 1961.

[18] A. Desio, E.G. Mancini, On the Geology of the Southern Slope of the Masherbrum Peak and the Upper Hushe Valley (Karakorum, Central Asia), Atti Accad. Naz. Lincei Mem. VIII (XII) (1974) 7–99.

[19] B. Zanettin, Geology and Petrology of Haramosh-Mango Gusor area, Scientific reports of Italian Expedition of the Karakorum and Hindu Kush, A. Desio Leader, III (I), F.J. Brill, Leiden, 1964.

[20] A. Zanchi, M. Gaetani, S. Poli, The Rich Gol Metamorphic Complex; evidence of separation between hindu Kush and Karakorum (Pakistan), C. R. Acad. Sci. Paris 325 (1997) 877–882.

[21] A. Zanchi, Structural evolution of the North Karakorum cover, North Pakistan, in: P.J. Treloar, M.P. Searle (Eds.), Himalayan Tectonics, Geol. Soc. London, Spec. Publ. 74 (1993) 21–38.

[22] M. Gaetani, The Karakorum Block in Central Asia, from Ordovician to Cretaceous, Sediment. Geol. 109 (1996) 339–359.

[23] K.A. Kafarskyi, J. Abdullah, Tectonics of north-east Afghanistan (Badakhstan, Wakhran, Nurestan) and relationship with the adjacent territories, Atti Convegni Lincei Roma 21 (1976) 87–113.

[24] M. Buchroithner, H. Gamerith, On the Geology of the Tirich Mir area, Central Hindu Kush (Pakistan), Jahrb. Geol. Bundesanst. 128 (1986) 367–381.

[25] A. Desio, Geographical features of the Karakorum. Italian expedition Karakorum and Hindu Kush, Univ. Milano, 1992.

[26] V.C. Takhur, D.K. Misra, Tectonic framework of the Indus and Shyok suture zones in eastern Ladakh (N-W Himalaya), Tectonophysics 101 (1984) 207–220.

[27] H. Rai, Geology of the Nubra Valley and its significance on the evolution of the Ladakh Himalaya, in: V.C. Thakur, K.K. Sharma (Eds.), Geology of Indus Suture Zone of Ladakh, Wadia Institute of Himalayan Geology, Dehra Dun, 1983, pp. 79–97.

[28] M.P. Searle, R.F. Weinberg, W.J. Dunlap, Transpressional tectonics along the Karakoram fault zone, Northern Ladakh: constraints on Tibetan extrusion, Geol. Soc. London, Spec. Pub. 135 (1998) 307–326.

[29] M. Gaetani, G. Gosso, U. Pognante, A geological transect from Kun Lun to Karakorum (Sinkiang, China): the western termination of the Tibetan Plateau, Preliminary note. Terra Nova 2 (1990b) 23–30.

[30] D.L. Sun, On the permian biogeographic boundary between Gondwana and Eurasia in Tibet, China as the eastern section of the Tethys, Paleogeogr. Palaeoclimatol. Palaeoecol. 100 (1993) 59–77.

[31] R.A.K. Tahirkeli, M. Mattauer, F. Proust, P. Tapponnier, The India Eurasia suture zone in Northern Pakistan: Synthesis and interpretation of recent data at plate scale, in: A. Farah, K.A. De Jong (Eds.), Geodynamics of Pakistan, Geol. Surv. Pakistan, Quetta, 1979, pp. 125–130.

[32] C.R. Hanson, The northern suture in the Shigar valley, Baltistan, northern Pakistan, Geol. Soc. Am. Spec. Paper 232 (1989) 203–215.

[33] P.J. Treloar, D.C. Rex, P.G. Guise, M.P. Coward, M.P. Searle, B.F. Windley, M.G. Petterson, M.Q. Jan, I.W. Luff, K-Ar and Ar-Ar geochronology of the Himalayan collision in NW Pakistan: constraints on the timing of suturing, deformation, metamorphism and uplift, Tectonics 8 (1989) 884–909.

[34] Y. Rolland, A. Pêcher, C. Picard, Mid-Cretaceous Back-arc formation and Arc evolution along the Asian margin: the Shyok Suture Zone in northern Ladakh (NW Himalaya), Tectonophysics 325 (2000) 145–173.

[35] F. Debon, P. Le Fort, D. Dautel, J. Sonet, J.L. Zimmermann, Granites of western Karakorum and and northern Kohistan (Pakistan): a composite Mid-Cretaceous to upper Cenozoic magmatism, Lithos 20 (1987) 19–40.

[36] A. Desio, E. Martina, P. Spaeda, A. Notrapertro, Geology of the Chogo Lungma-Biafo-Hispa area, Karakorum (NW Pakistan), Atti Accad. Naz. Lincei Mem. XVIII (II) (1985) 1–53.

[37] A. Desio, Geological tentative map of the Western Karakorum, Scale: 1/500 000, Instituto Geol. Univ. Milano, Milano, 1964.

[38] M.P. Searle, R. Tirrul, Structural and thermal evolution of the Karakoram crust, Journal of the Geological Society of London 148 (1991) 65–82.

[39] S. Tonarini, I.M. Villa, F. Oberli, M. Meier, D.A. Spencer, U. Pognante, J.G. Ramsay, Eocene age of eclogite metamorphism in Pakistan Himalaya: implications for India-Eurasia collision, Terra Nova 5 (1993) 13–20.

[40] J. de Sigoyer, V. Chavagnac, J. Blichert-Toft, I.M. Villa, S. Guillot, B. Luais, M. Cosca, G. Mascle, Dating the Indian continental subduction and collisional thickening in the northwest Himalaya: Multichronology of the Tso Morari eclogites, Geology (2000) 487–490.

[41] R.P. Parrish, R. Tirrul, U-Pb ages of the Baltoro granite, northwestern Himalaya, and implications for zircon inheritance and monazite U-Pb systematics, Geology 17 (1989) 1076–1079.

[42] J. Fraser, M.P. Searle, R. Parrish, S. Noble, U-Pb geochronology on the timing of metamorphism and magmatism in the Hunza Karakoram, (abstract), Terra Nostra 99 (2) (1999) 45–46.

[43] U. Schärer, P. Copeland, T.M. Harrison, M.P. Searle, Age, cooling history and origin of post-collisional leucogranites in the Karakoram batholith: A multi-system isotope study, N. Pakistan. Journal of Geology 98 (1990) 233–251.

[44] I.M. Villa, Y. Lemmenicier, P. Le Fort, Late Miocene to Early Pliocene tectonometamorphism and cooling in south-central Karakorum and Indus-Tsangpo suture, Chogo Lungma area (NE Pakistan), Tectonophysics 260 (1996) 201–214.

[45] E. Belluso, R. Ruffini, M. Schaller, I.M. Villa, Electron-microscope and Ar isotope characterization of chemically heterogeneous amphiboles from the Palala shear zone, Limpopo Belt, South Africa. Eur. J. Mineral. 12 (2000) 45–62.

[46] I.M. Villa, J. Hermann, O. Müntener, V. Trommsdorff, 39Ar-40Ar dating of multiply zoned amphibole generations (Malenco, Italian Alps). Contrib. Mineral. Petrol., accepted.

[47] S.S. Sun, W.F. McDonough, Chemical and isotopic systematics of oceanic basalts: implications for mantle composition and processes, in: A.D. Saunders, M.J. Norry (Eds.), Magmatism in Ocean Basins, Geol. Soc. London. Spec. Pub. 42 (1989) 313–345.

[48] R.W. Kay, Aleutians magnesian andesites: melts from subducted Pacific Ocean crust, J. Volcanol. Geotherm. Res. 4 (1978) 117–132.

[49] R. Shinjo, Geochemistry of high-Mg andesites and the tectonic evolution of the Okinawa Trough-Ryukyu arc system, Chem. Geol. 157 (1999) 69–88.

[50] H. Martin, The mechanisms of petrogenesis of the Archean continental crust - Comparison with modern processes, Lithos 30 (1999) 373–388.

[51] M.J. Defant, M.S. Drummond, Derivation of some modern arc magmas by melting of young subducted lithosphere, Nature 347 (1990) 662–665.

[52] F.G. Sajona, R.C. Maury, H. Bellon, J. Cotten, M. Defant, High Field Strength Element enrichment of Pliocene-Pleistocene Island Arc Basalts, Zamboanga Peninsula, Western Mindanao (Philippines), J. Petrol. 37 (1996) 693–725.

[53] H. Martin, Effect of steeper Archean geothermal gradient on geochemistry of subduction-zone magmas, Geology 14 (1986) 753–756.

[54] J. Veizer, A. Davin, K. Azmy, P. Bruckschen, D. Buhl, F. Bruhn, G. Carden, A. Diener, S. Ebneth, Y. Godderis, T. Jasper, C. Korte, F. Pawellek, O.G. Podlaha, H. Strauss, $^{87}Sr/^{86}Sr$, $\delta^{13}C$ and $\delta^{18}O$ evolution of Phanerozoic seawater, Chemical Geology 161 (1999) 59–88.

[55] L.A. Derry, A.J. Kaufman, B.J. Stein, Sedimentary cycling and environmental change in the Late Proterozoic : Evidence from stable and radiogenic isotopes, Geochimica Cosmochimica Acta 56 (1992) 1317–1329.

[56] P.I. Nabelek, T.C. Labotka, J.R. O'Neil, J.J. Rapike, Contrasting fluid-rock interaction between Notch granite intrusion and argillites and limestones in western Utah : evidence from stable isotopes and phase assemblages, Contrib. Mineral. Petrol. 86 (1984) 25–34.

[57] R.G. Coleman, Ophiolites: ancient oceanic lithosphere? Springer, New York, 1977.

[58] A. Nicolas, Structures of ophiolites and dynamics of oceanic lithosphere, Kluwer, Dordrecht, 1989.

[59] P.K. Kepezhinskas, R.N. Taylor, H. Tanaka, Geochemistry of plutonic spinels from the Kamchatka arc: comparisons with spinels from other tectonic settings, Mineralogical Magazine 57 (1993) 575–589.

[60] S. Arai, Chemistry of chromian spinel in volcanic rocks as a potential guide to magma chemistry, Mineralogical Magazine 56 (1992) 173–184.

[61] M.Q. Jan, B.F. Windley, Chromian-spinel silicate geochemistry in ultramafic rocks of the Jijal Complex, northwest Pakistan, J. Petrol. 31 (1990) 667–715.

[62] B. Orberger, J.P. Lorand, J. Girardeau, J.C.C. Mercier, E.S. Pitragool, Petrogenesis of ultramafic rocks and associated chromitites in the Nan Uttaradit ophiolite, northern Thailand, Lithos 35 (1995) 153–182.

[63] H.J.B. Dick, T. Bullen, Chromian spinel as a petrogenetic indicator in abyssal and alpine-type peridotites and spatially associated lavas, Contrib. Mineral. Petrol. 86 (1984) 54–76.

[64] I.J. Parkinson, J.A. Pearce, Peridotites from the Izu-Bonin-Mariana forearc (ODP Leg 125): Evidence for mantle melting and melt-mantle interaction in a supra-subductive zone setting, J. Petrol. 39 (1998) 1577–1618.

[65] T. Ishii, P.T. Robinson, H. Maekawa, R. Fiske, Petrological studies of peridotites from diapiric serpentinites seamounts in the Izu-Ogasawara-Mariana forearc, Leg 125: Scientific results, Volume 125: College Station, Texas, Ocean Drilling Program, 1982, pp. 445–463.

[66] N.M. Evensen, P.J. Hamilton, R.K. O'Nions, Rare earth abundances in chondritic meteorites, Geochim. Cosmochim. Acta. 42 (1978) 1199–1212.

[67] J.M. Brenan, H.F. Shaw, F.J. Ryeson, D.L. Phiney, Mineral-aqueous fluid partitioning of trace elements at 900°C and 2.0 GPa: constrains on the trace element chemistry of mantle and deep crustal fluids, Geochim. Cosmochim. Acta 59 (1995) 3331–3350.

[68] H. Keppler, Constrains from partitioning experiments on the composition of subduction-zone fluids, Nature 380 (1996) 52–57.

[69] T. Kogiso, Y. Tatsumi, S. Nakano, Trace element transport during dehydration processes in the subducted oceanic crust. 1, experiments and implications for the origin of ocean island basalts, Earth Planet. Sci. Lett. 148 (1997) 193–205.

[70] R.W. Kay, Elemental abundancies relevant to identification of magma sources, Philos. Trans. R. Soc. London Ser. A 310 (1984) 535–547.

[71] M.T. McCulloch, J.A. Gamble, Geochemical and geodynamical constrains on subduction zone magmatism, Earth Planet. Sci. Lett. 102 (1991) 358–374.

[72] J. Tarney, A. Saunders, D.P. Mattey, D.A. Wood, N.G. Marsh, Geochemical aspects of back-arc spreading in the Scotia Sea and western Pacific, Phil Trans. R. Soc. London A297 (1981) 179–202.

[73] A.D. Saunders, J. Tarney, Geochemical characteristics of basaltic volcanism within back-arc basins, in: B.P. Kokelaar, M.F. Howells (Eds.), Marginal Basin Geology, Geol. Spec. Pub. 16 (1984) 59–76.

[74] A.M. Volpe, J.D. Macdougall, J.W. Hawkins, Mariana Trough basalts (MTB): trace element and Sr-Nd isotopic evidence for mixing between MORB-like and Arc-like melts, Earth. Planet. Sci. Lett. 82 (1987) 241–254.

[75] J.A. Pearce, Trace element characteristics of lavas from destructive plate boundaries, in: R.S. Thrope (Ed.), Andesites: Orogenic Andesites and Related Rocks, J. Wiley and sons, Chichester, 1982, pp. 525–548.

[76] M. Nohara, K. Hirose, J.P. Eissen, T. Urabe, M. Joshima, The North Fiji Basin basalts and their magma sources: Part II. Sr-Nd isotopic and trace element constrains, Marine Geology 116 (1994) 179–195.

[77] J.P. Eissen, M. Nohara, J. Cotten, K. Hirose, North Fiji basin basalts and their magma sources: Part I. Incompatible element constrains, Marine Geology 116 (1994) 153–178.

[78] D.W. Peate, J.A. Pearce, C.J. Hawkesworth, H. Colley, C.M.H. Edwards, K. Hirose, Geochemical variations in Vanuatu Arc lavas: the role of subducted material and a variable mantle wedge composition, J. Petrol. 10 (1997) 1331–1358.

[79] Y. Rolland, C. Picard, A. Pêcher, H. Lapierre, D. Bosch, F. Keller, The Cretaceous Ladakh Arc of NW Himalaya - Slab melting and melt-mantle interaction during fast northward drift of Indian Plate, Chem. Geol. (2002) 139–178.

[80] A. Zindler, S. Hart, Chemical geodynamics, Ann. Rev. Earth Planet. Sci. 14 (1986) 493–571.

[81] W.M. White, A.W. Hofmann, H. Puchelt, Isotope geochemistry of Pacific mid-ocean ridge basalt, J. Geophys. Res 92 (1987) 4881–4893.

[82] D. Ben Othman, W.M. White, J. Patchett, The geochemistry of marine sediments, island arc magma genesis and crust-mantle recycling, Earth Planet. Sci. Lett. 94 (1989) 1–21.

[83] C.J. Hawkesworth, K. Gallagher, J.M. Hergt, F. McDermott, Destructive plate margin magmatism: geochemistry and melt generation, Lithos 33 (1994) 169–188.

[84] C. Class, D.M. Miller, S.L. Goldstein, C.H. Langmuir, Distinguishing melt and fluid subduction components in Umnak Volcanics, Aleutian arc, Geochem. Geophys. Geosyst. 1 (1999GC000010). Geochem. Geophys. Geosyst. 1 (1999GC000010). http://gcubed.magnet.fsu.edu/publications/articles, 2000.

[85] M. Gaetani, G. Gosso, U. Pognante, A geological transect from Kun Lun to Karakorum (Sinkiang China): the western termination of the Tibetan Plateau. Preliminary note, Terra Nova 2 (1990) 23–30.

[86] R. Xu, U. Schärer, C.J. Allègre, Magmatism and metamorphism in the Lhasa Block (Tibet): A geochronological study, J. Geol. 93 (1985) 41–57.

[87] J.X. Yin, J.T. Xu, C.G. Liu, H. Li, The Tibetan Plateau: regional stratigraphic context and previous work, in: C.F. Chang, et al (Eds.), The geological evolution of Tibet. Roy. Soc. London Phil. Trans. 327 (1988) 5–52.

[88] J. Besse, V. Courtillot, Paleogeographic maps of the continents bordering the Indian Ocean since the Early Jurassic, J. Geophys. Res. 93 (1988) 11791–11808.

[89] A.M.C. Sengör, B.A. Natal'in, Paleotectonics of Asia: fragments of a synthesis, in: A. Yin, M. Harisson (Eds.), The tectonic evolution of Asia, Cambridge Univ. Press, 1996, pp. 486–640.

[90] A. Zanchi, S. Poli, P. Fumagalli, M. Gaetani, Mantle exhumation along the Tirich Mir Fault Zone, NW Pakistan: pre-mid-Cretaceous accretion of the Karakoram terrane to the Asian margin, in: M.A. Khan, P.J. Treloar, M.P. Searle, M.Q. Jan (Eds.), Tectonics of the Nanga Parbat Syntaxis and the Western Himalaya. Geol. Soc. London Spec. Pub. 170 (2000) 237–252.

[91] N.I. Volkova, V.I. Budanov, Geochemical discrimination of metabasalt rocks of the Fan-Karategin transitional blueschist / greenschist belt, South Tianshan, Tajikistan: seamount volcanism and accretionary tectonics, Lithos 47 (1999) 201–216.

[92] Pan, Yusheng, A preliminary study on the regionalization in the western Kunlun mountain region, J. Nation. Resource 4 (3) (1989) 222–227.

[93] P. Matte, P. Tapponnier, N. Arnaud, L. Bourjot, J.P. Avouac, P. Vidal, Liu Qing, Pan Yusheng, Wang Yi, Tectonics of Western Tibet, between the Tarim and the Indus, Earth Planet. Sci. Lett. 142 (1996) 311–330.

[94] Gao Jun, Li Maosong, Xiao Xuchang, Tang Yaoqing, He Guoqi, Paleozoic tectonic evolution of the Tianshan Orogen, northwestern China, Tectonophysics 287 (1998) 213–231.

[95] K. Cui, Studies on the structural deformation and ductile shear zones of the Western Tianshan, Ph.D. Thesis, Nanjing Univ., 1995.

[96] F. Xue, M.F. Lerch, A. Kröner, T. Reischmann, Tectonic evolution of the East Qinling Mountains, China, in the Palaeozoic: a review and new tectonic model, Tectonophysics 253 (1996) 271–284.

[97] F. Rolfo, B. Lombardo, R. Compagnoni, P. Le Fort, Y. Lemmenicier, A. Pêcher, Geology and metamorphism of the Ladakh Terrane and Shyok Suture Zone in the Chogo Lungma - Turmik area (northern Pakistan), Geodinamica Acta 10 (1997) 251–270.

[98] P.D. Clift, J.E. Dixon, Jurassic ridge collapse, subduction initiation and ophiolite obduction in the southern Greek Tethys, Eclogae geol. Helv. 91 (1998) 128–138.

[99] T.H. Trosvik, P.D. Ryan, A. Trench, D.A.T. Harper, Cambrian-Ordovician paleogeography of Baltica, Geology 19 (1991) 7–10.

[100] I.W.D. Dalziel, On the Organization of American plates in the Neoproterozoic and the breakout of Laurentia, GSA Today 2 (11) (1992) 237–241.

[101] M.A. Smethurst, A.N. Khramov, T.H. Torsvik, The Neo-proterozoic and Palaeozoic palaeomagnetic data for the Siberia Platform: from Rodinia to Pangea, Earth Sci. Rev. 43 (1998) 1–24.

[102] Baochun Huang, Zhenyu Yang, Yo-ichiro Otofuji, Rixiang Zhu, Early Paleozoic paleomagnetic poles from the western part of the North China Block and their implications, Tectonophysics 308 (1999) 377–402.

[103] J.A. Barrat, F. Keller, J. Amossé, R.N. Taylor, R.W. Nesbitt, J. Hirata, Determination of rare earth elements in sixteen silicate samples by ICP-MS after Tm addition and Im exchange separation, Geostand. Newslett. 20 (1996) 133–139.

[104] H. Lapierre, V. Dupuis, B. Mercier de Lépinay, M. Tardy, M. Ruiz, R.C. Maury, J. Hernandez, M. Loubet, Is the lower Duarte Igneous Complex (Hispaniola) a remnant of the Caribean plume-generated oceanic plateau? J. Geol. 105 (1999) 111–120.

[105] A.M. Aucour, S.M.F. Sheppard, O. Guyomar, J. Wattelet, Use of ^{13}C to trace origin & cycling of inorganic carbon in the Rhône river system, Chemical Geology 159 (1999) 87–105.